

X-ray Observations of Neutron Stars and Pulsars: First Results from XMM-Newton

W. Becker, B. Aschenbach

Max-Planck-Institut für extraterrestrische Physik, Giessenbachstraße, 85741 Garching, Germany

Abstract. The X-ray Multi-Mirror Mission XMM-Newton is ESA's largest observatory so far; it is dedicated to explore the Universe in the 0.2 – 15 keV X-ray band of the electromagnetic spectrum. Because of its large collecting area very faint sources not accessible before can be observed and it is therefore the long awaited instrument to study young pulsars and neutron stars in supernova remnants, cooling neutron stars and millisecond pulsars at X-ray energies. The high throughput of the instruments, which all are operated simultaneously, provide high resolution spectral, spatial and temporal information from a source during a single observation and make XMM-Newton unique and best suited for pulsar studies. In this article we briefly describe the instrument capabilities useful for pulsar observations and provide information on the timing accuracy on the relative and absolute scale. We further provide scientific results from observations of the Crab-pulsar, PSR J1617-5055 near RCW 103, of young neutron stars in the supernova remnants RX J0852-4622, Puppis-A and RCW 103 including 1E161348-5055.1 which is identified to be the second binary in a supernova remnant. In addition we report on observations of the cooling neutron star PSR B1055-52 and on the millisecond pulsar PSR J0030+0451 which all were observed by XMM-Newton during the first two years of scientific operation.

cluded any broad band study of the pulsar emission. Any conclusive identification of the nature of the 'hard tails' indicated in various X-ray spectra of cooling neutron stars and ms-pulsars was therefore not possible. ASCA and the Narrow Field Instruments on BeppoSAX, on the other hand, were sensitive up to 10 keV and were very successful in discovering young neutron stars in SNRs by their hard X-ray emission (cf. Torii 1998; Saito 1998). The lack of high resolution imaging, however, did in most cases not allow to resolve any central compact X-ray source from the surrounding plerion or supernova remnant.

The expectations from an observatory like XMM-Newton, with its enormous collecting area, multi-instrumentation and wide energy bandwidth are therefore high, especially in the field of neutron star astronomy where the targets (apart from a few Crab-like objects) are known to be relatively faint X-ray emitters.

XMM carries three identical X-ray telescopes, each of which is equipped with an X-ray CCD camera in the focal planes, called EuroPan Imaging Camera (EPIC). Two of the cameras are constructed using Metal Oxide Semiconductor technology (MOS1 & MOS2) and the third camera is built in Positive-Negative depleted Silicon Semiconductor technology, therefore called PN-camera. About half of each of the beams of the two telescopes operating with the MOS's is intercepted by Reflection Grating Spectrometers (RGS1 & RGS2), which diffract the X-rays to two dedicated CCD detectors. Optical observations can be made with a separate co-aligned optical telescope called Optical Monitor (OM). The instruments can be operated in parallel and they provide various observation modes which are very well suited for pulsar studies. Table 1 summarizes the timing modes available for the PN and MOS detectors. Also listed are the detectors' field of view (in units of detector pixels and angular units) and the associated temporal resolution. Useful is the PN small-window mode which provides imaging information for a sky field of $\sim 4.4' \times 4.4'$ along with spectral and a ~ 6 ms temporal resolution. This mode has its benefit for timing studies of sources located in crowded regions or in supernova remnants. It prevents source confusion which often is found to be the limiting factor when using the faster timing modes.

1. Introduction

X-ray observatories like ROSAT, ASCA, BeppoSAX and RXTE have achieved an important progress in neutron star and pulsar astronomy. The identification of Geminga and of cooling neutron stars (Halpern & Holt 1992; Ögelman 1995 and references therein), the discovery of pulsed X-ray emission from millisecond pulsars (Becker & Trümper 1993) and of the first accreting X-ray ms-pulsar SAX J1808.4-3658 (in't Zand et al. 1998; Wijnands & van der Klis) are only a few of the fascinating results. ROSAT's predominant contribution was due to its favorable soft response down to 0.1 keV, which permitted to observe the very soft thermal emission from the neutron stars' surface, but the relatively small bandwidth of up to 2.5 keV pre-

Table 1. Instrument modes available on XMM-Newton for timing studies of pulsars. The image size is given in detector pixels and angular units. FOV is the full field of view.

EPIC PN Mode	Image size / pixel /	FOV arcmin	Temporal resolution
Small window	2D - 64×64	$4.4' \times 4.4'$	5.67 ms
Fast-timing	1D - 64×199	$4.4' \times 13.75'$	0.02956 ms
Burst	1D - 64×199	$4.4' \times 13.75'$	0.0072 ms

EPIC MOS Mode	Image size / pixel /	FOV arcmin	Temporal resolution
part. window1	2D - 100×100	$1.8' \times 1.8'$	200 ms
part. window2	2D - 300×300	$5.5' \times 5.5'$	700 ms
timing	1D - user defined pixel area		≥ 1.5 ms

Note: In PN timing modes only CCD #4 (of 12 CCDs in total) is active whereas in MOS timing modes only the central CCD provides timing information and the remaining 6 chips are operated in imaging mode. Burst mode is designed for very bright sources up to 6.3 Crab only. The efficiency of the PN small-window mode is $\sim 30\%$ of that of the PN timing mode. In burst mode it is only 3%. XMM's spatial resolution is $\sim 15''$ (HEW). The size of a CCD pixel is $1.1'' \times 1.1''$ and $4.125'' \times 4.125''$ for the MOS and PN camera, respectively.

For the PN fast-timing and burst modes the spatial and spectral information from a 64×199 CCD pixel array is condensed into a one dimensional 64×1 pixel array (1D-image), i.e. the spatial information in Y-direction is lost due to the continuous read-out of the CCD. In these modes, the complete photon flux (source plus DC emission from foreground or background sources located along the read-out direction) is accumulated and collapsed in the final 1D-image, severely reducing the signal-to-noise ratio and preventing the detection of X-ray pulsations from the target of interest. Soft-proton flares which are known to happen on various time scales and frequencies almost unpredictable can likewise produce enough DC flux to prevent the detection of X-ray pulsations from a pulsar of intermediate X-ray brightness if the fast-timing mode was selected for the observation. For pulsars with periods longer than ~ 60 ms, the PN small-window mode is a good choice even in view of a $\sim 30\%$ reduced efficiency compared with the fast-timing mode. For millisecond pulsar observations, however, the fast-timing mode is the only one which provides sufficient temporal resolution for timing studies.

The strong interest in XMM-Newton, especially for neutron star and pulsar research, is supported by the large list of sources accepted for observations in AO1 (cf. Table 2). The proposed science and accepted targets cover a wide range of different categories, from young pulsars in supernova remnants to cooling neutron stars, binary-pulsars, old but nearby pulsars and millisecond pulsars.

Even a small survey for potentially X-ray bright rotation-powered pulsars is included.

In the following sections we will report on the first XMM observations of pulsars, browsing through the various categories from young Crab-like pulsars and neutron star candidates in supernova remnants to the very old millisecond pulsars, summarizing the most exciting results. Before we do so, however, we will briefly review the various emission processes discussed to be the source for the observed X-ray emission.

2. High-energy X-ray Emission Processes

As a result of observations with the satellite observatories ROSAT, ASCA and Chandra, the number of rotation-powered pulsars seen at X-ray energies has reached 51 (as of June 2002). Almost half of the detected pulsars are ms-pulsars. Several of these objects have been detected at optical wavelengths and at gamma-ray energies (cf. Tab.3 and Tab.4 for a summary), advocating for multi-wavelength studies of the pulsar emission. This approach is of great benefit as the physical processes which cause the emission in different wavelength bands are obviously related to each other. Although the quality of the data obtained with different instruments and/or in different wavebands is inevitably rather inhomogeneous, and the conclusions drawn on these data are to some extent unlikely to be solid in a number of cases, there is general consensus that the X-radiation detected from rotation-driven pulsars has to be attributed to various thermal and non-thermal emission processes including the following:

- Non-thermal emission from charged relativistic particles accelerated in the pulsar magnetosphere. This emission is characterized by power-law like spectra over a broad energy band. The emitted radiation can be observed from the optical to the gamma-ray band.
- Extended emission from pulsar-driven synchrotron nebulae. Depending on the local conditions (e.g., matter density of the ambient medium), these nebulae can be observed from radio through hard X-ray energies.
- X-ray and gamma-ray emission from interaction of relativistic pulsar winds with a close companion star or with the wind of a companion star.
- Photospheric emission from the hot surface of a cooling neutron star. In this case a modified black-body spectrum and smooth, low-amplitude intensity variations with the rotational period are expected, observable from the optical through the soft X-ray range.

In many pulsars the observed X-ray emission is due to a mixture of different thermal and non-thermal processes. The available data do not always allow to discriminate between the different emission scenarios. This was true for

Table 2. List of Pulsars which are accepted for observations by XMM-Newton during AO1. Also listed is the main instrument (PN, MOS, RGS or OM) and the proposed exposure time in ksec. CAL indicates calibration targets which are observed at regular time intervals for calibration purposes and in various instrument modes and setups. *obs* indicates whether a target has been observed by June 2002. Category C-Targets are supposed to be optional and not guaranteed to be observed.

Young Pulsars	Status	Instrument	Exposure	Cooling NS	Status	Instrument	Exposure
PSR B0531+21	obs	EPIC PN/MOS	CAL	PSR B0656+14	obs	EPIC PN/MOS	40
PSR 0540-69	obs	EPIC PN/MOS	CAL	Geminga	obs	EPIC RGS	40
PSR 1509-58	obs	EPIC PN/MOS	20	PSR B1055-52	obs	EPIC PN/MOS	80
PSR B0833-45	obs	EPIC RGS	90	PSR J0358+5413	obs	EPIC PN/MOS	30
PSR B1811-19	obs	EPIC PN/MOS	30	PSR J0538+2817		EPIC PN/MOS	20
PSR J0537-6909	obs	EPIC PN/MOS	40	Old nearby NS			
PSR J1709-4428	obs	EPIC PN/MOS	90	PSR B1929+10		EPIC PN/MOS	35
PSR B1016-58		EPIC PN/MOS	30	PSR 0950-08		EPIC PN/MOS	100
PSR B1823-13	obs	EPIC PN/MOS	55	PSR B0823+26	obs	EPIC PN/MOS	50
PSR J1119-6127		EPIC PN/MOS	C60	PSR J1908+0734		EPIC PN/MOS	C30
PSR B1800-21		EPIC PN/MOS	C40	PSR J2043+2740		EPIC PN/MOS	20
ms-Pulsars				Mini Survey			
PSR J0030+0453	obs	EPIC PN/MOS	30	PSR B0136-57		EPIC PN/MOS	5
PSR J0437-4715		EPIC PN/MOS	70	PSR B0540-23		EPIC PN/MOS	5
PSR J1024-0719		EPIC PN/MOS	80	PSR B0611-22	obs	EPIC PN/MOS	5
PSR J2124-3358	obs	EPIC PN/MOS	70	PSR J0631+1036	obs	EPIC PN/MOS	5
PSR J0218+42	obs	EPIC PN/MOS	35	PSR B0740-28	obs	EPIC PN/MOS	5
PSR J1012+53	obs	EPIC PN/MOS	20	PSR B0906-49	obs	EPIC PN/MOS	5
PSR J0034-0534	obs	EPIC PN/MOS	30	PSR B1221-63		EPIC PN/MOS	5
PSR J0751+18	obs	EPIC PN/MOS	40	PSR B1449-64	obs	EPIC PN/MOS	5
Binary Pulsars				PSR B1634-45	obs	EPIC PN/MOS	5
PSR B1259-63	obs	EPIC PN/MOS	10	PSR B1719-37	obs	EPIC PN/MOS	5
PSR B1259-63	obs	EPIC PN/MOS	10	PSR B1742-30	obs	EPIC PN/MOS	5
PSR B1259-63	obs	EPIC PN/MOS	10	PSR J1757-2421	obs	EPIC PN/MOS	5
PSR B1259-63	obs	EPIC PN/MOS	10	PSR B1757-244		EPIC PN/MOS	5
PSR B1259-63		EPIC PN/MOS	10	PSR J0117+5914		EPIC PN/MOS	5
PSR B1259-63		EPIC PN/MOS	10	PSR J1705-1906		EPIC PN/MOS	5
PSR B1259-63		EPIC PN/MOS	10	PSR J1730-3350		EPIC PN/MOS	5
PSR B1259-63		EPIC PN/MOS	10	PSR J1825-0935		EPIC PN/MOS	5
PSR B1259-63		EPIC PN/MOS	10	PSR J1856+0113		EPIC PN/MOS	5

ROSAT and ASCA observations and might still be true for Chandra and XMM data.

It is well established, however, that magnetospheric emission from charged particles, accelerated in the neutron star magnetosphere along the curved magnetic field lines, dominates the radiation from young *rotation-powered* pulsars with ages $\lesssim 5000$ years. Middle aged pulsars such as the three Musketeers PSR B0656+14, PSR B1055-52 and Geminga are seen to have composite spectra consisting of two or three components which are a soft thermal (cooling) and a hotter polar-cap component as well as some hard emission associated with non-thermal processes (cf. §4). For the millisecond pulsars, ROSAT and ASCA did not allow to conclusively clarify whether their emission is purely due to the presence of hot/heated polar-caps, due to non-thermal magnetospheric emission or a mixture of both or whether there exists even a dichotomy

among the emission properties which correlates with the pulsar's spin-parameters. Chandra and XMM-Newton observations of the two ms-pulsars PSR J0437-4715 and PSR J0030+0451 (cf. §5) as well as the detection of 11 ms-pulsars in the Globular Cluster 47TUC seem to suggest that both, a thermal and a non-thermal emission component are present in all ms-pulsars though it is difficult to accomplish the gross similarity between the radio and X-ray pulse profiles with these two (or even more) different components at work.

3. Young Neutron Stars in Supernova Remnants

3.1. The Crab- and Vela-like Pulsars

The majority of the young Crab- and Vela-like pulsars have been observed by XMM-Newton during AO1 with the aim to study the pulsars' temporal emission proper-

ties along with a study of the pulsars' wind nebulae or a search for it. While a large fraction of data was delivered to the PIs only recently and are still in the process of data analysis, the Crab, PSR 0540-69 and PSR 1509-58 were observed for the purpose of instrument calibration (clock and mirrors), and have undergone a first scientific analysis already.

Although the Crab has been observed with almost every instrument since its discovery, it is amazing to see how many new results were obtained with Chandra and XMM-Newton. First images taken with the Advanced CCD Imaging Spectrometer (ACIS) aboard Chandra have already provided spectacular details of the inner nebula structure associated with the pulsar-wind outflow — in addition to the torus ($r \approx 0.38$ pc) the *inner ring* ($r \approx 0.14$ pc), *jet* and *counter-jet* have been identified (Weisskopf et al. 2000). In the same observation, systematic variations of the X-ray spectrum were discovered throughout the nebula. A more detailed study of the spectral variations became possible with the XMM data, taken in March 2000 with the EPIC detectors (Willingale et al. 2001). Figure 1 shows an X-ray image of the Crab nebula in which the color coding is associated with the photon-index α of the nebula's X-ray spectrum, $dN/dE \propto E^{-\alpha}$. This image impressively illustrates the different shape of the spectra of the torus ($\alpha = 1.8 \pm 0.006$), the jet ($\alpha = 2.1 \pm 0.013$) and the outer nebula regions ($\alpha = 2.34 \pm 0.006$). Similar results were obtained by Chandra, measuring the hardness ratio distribution throughout the nebula (Weisskopf et al. 2000). For the pulsar, a photon spectral index of $\alpha = 1.63 \pm 0.09$ is determined from out-of-time events selected along the read-out direction of the CCDs, and thus not affected by pile-up. The spectral difference between the jet and the torus is found to be likely due to an intrinsically steeper electron spectrum of the jet. The outer regions of the nebula show the steepest spectrum, which is likely to be due to enhanced synchrotron losses of the electrons during their ride from the pulsar to the outskirts (Willingale et al. 2001).

Observations with the High Resolution Imager (HRI) aboard ROSAT has already shown that at least $\sim 75\%$ of the Crab-pulsar's total soft X-ray flux is emitted from the co-rotating magnetosphere (Becker & Trümper 1997). Recent observations with the High Resolution Camera aboard Chandra by Tennant et al. (2001) at an angular resolution of ≤ 1 arcsec has improved this number in showing that in the 0.5 – 10 keV band the pulsed fraction is $\sim 85\%$. The high pulsed fraction along with the monthly published radio ephemeris (Lyne et al., 2002) makes the Crab therefore an excellent target for the XMM-clock calibration. The Crab-pulsar was observed for that reason in March 2000, 2001 and 2002 with the PN in timing and burst mode, respectively. Because of the pulsar's brightness only the burst mode provides accurate spectral information not affected by pile-up effects, though the detector life time in that mode is only 3%. We have analyzed the

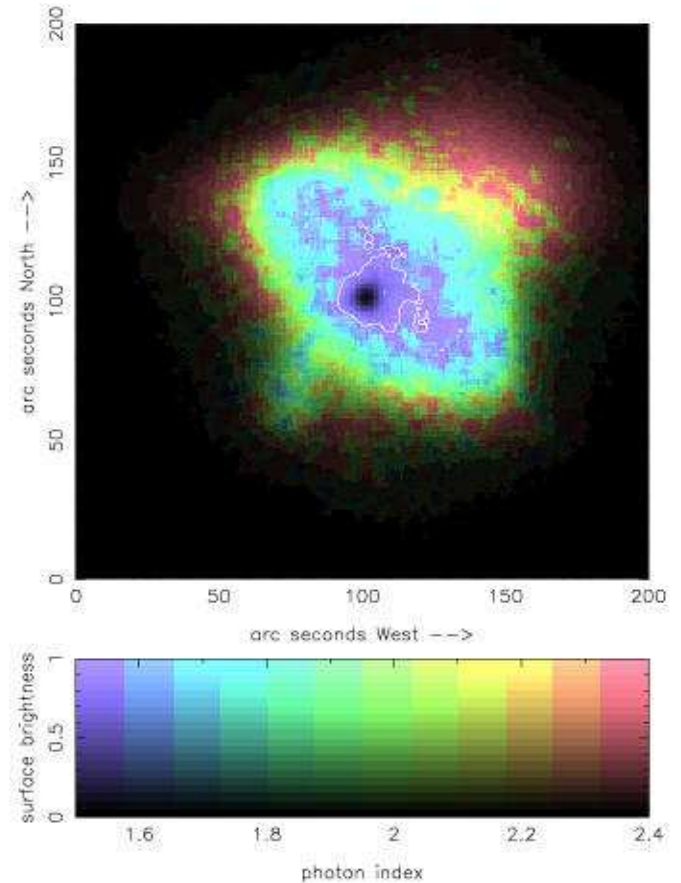


Fig. 1. The Crab as observed with the European Imaging Camera aboard XMM-Newton. The image has been spatially oversampled, using a bin size of 1 arcsec (instrument HEW ~ 15 arcsec). The color coding of surface brightness and photon index is shown in the lower panel. The white contour encircles the region compromised by pile-up. (From Willingale et al. 2001)

Crab data from all orbits (cf. Fig.2) and found that the pulsar period deduced from the XMM data matches to better than 2.5×10^{-10} s the radio period given in the Jodrell Bank monthly Crab ephemeris (Lyne et al., 2002). The difference is within the expected statistical uncertainty¹.

In addition to the relative timing we checked the accuracy of the XMM clock on the absolute scale by comparing the arrival time of the Crab pulsar's main peak with that measured in the radio band (Lyne et al., 2002). We find that for all XMM data the arrival of the main peak lead the arrival of the main radio peak by 0.047 ± 0.001 in phase (modulo the pulsar period), corresponding to a time dif-

¹ In previous versions of XMM-SAS the barycenter correction code was erroneous, leading to discrepancies of periods derived from EPIC data and compared to, e.g. radio ephemeris of up to $\Delta P/P = 7 \times 10^{-6}$ (Kuster et al. 2002). The code was fixed recently (SAS 5.3 and later versions) which improved the EPIC relative timing by three orders of magnitude.

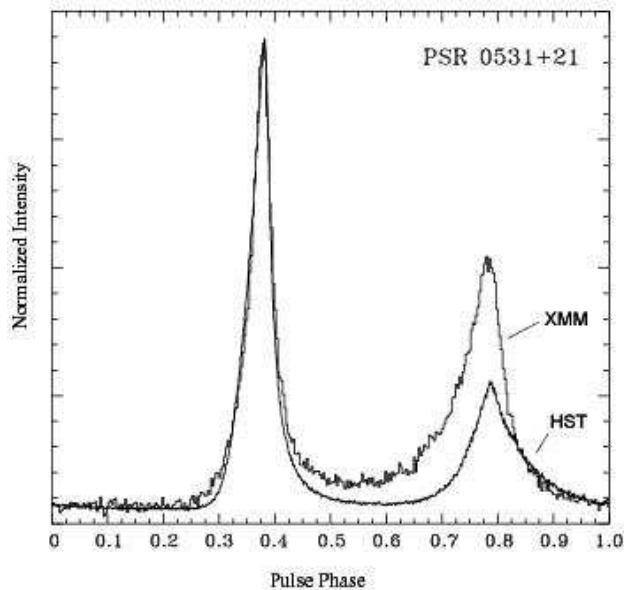


Fig. 2. The Crab pulse profile observed with the XMM-Newton and Hubble Space observatories. Peaks of the main pulse have been co-aligned in phase. A slight phase difference between the main and the second peaks is apparent which suggests a small energy dependence of the phase shift between main and secondary pulse peak.

ference of 1.57 ms (modulo the pulsar period). Rots et al. (2000) have analyzed all Crab data taken with RXTE since the start of the mission in January 1996 and found that the phase of the main X-ray peak is different from the radio peak by $\sim 300\mu\text{s}$. Depending on whether this phase difference observed in RXTE data is real or only reflects the accuracy of the RXTE timing, the phase alignment between radio and X-ray pulses measured by XMM is uncertain by 1.27 – 1.57 ms on the absolute scale. Careful analysis of all modules involved in XMM’s timing are currently in progress in order to improve the absolute clock accuracy.

Besides the Crab several other young pulsars have been observed by XMM during the first two years of scientific observations. One of these pulsars is PSR J1607 – 5055, which is a 69 ms pulsar located about 7 arcmin outside the boundary of the young supernova remnant RCW 103 (cf. Fig.9). The spin-down age of the pulsar is $\tau \sim 8000$ years (cf. Table 3) placing it among the youngest known radio pulsars. An association of RCW 103 and the pulsar was discussed but found to be unlikely (Dickel & Carter 1998; Kaspi et al. 1998). The pulsar distance is not very well constrained. The radio dispersion measure yields a distance of 6.1 – 6.9 kpc (Taylor & Cordes 1993) whereas Kaspi et al. (1998) conclude from a comparison between dispersion measure based distances and distances obtained from HI absorption measurements of PSR 1641-45 and PSR 1718-35 - which are both located within 20° of PSR

J1607–5055 - that the pulsar could be as close as ~ 4.5 kpc.

PSR J1607 – 5055 was discovered by its X-ray pulses in archival GINGA data (Torii et al. 1998). It was then detected also in the radio domain (Kaspi et al. 1998). With ASCA it was not possible to separate the pulsar from the close by RCW 103 supernova remnant, which limited modeling of the pulsar spectrum to energies > 3 keV (Torii et al. 2000). XMM-Newton has observed the pulsar in September 2001 for 30 ksec and for another 20 ksec but off-center because the target was RCW 103 (cf. §3.2). The XMM data of PSR J1617–5055 provide the first detailed pulsar spectrum in the 0.3 – 10 keV band. Among various spectral models a power-law spectrum with a photon index of $\alpha = 1.1 - 1.4$ (90% confidence range) is found to be the simplest but acceptable description of the spectrum up to 10 keV ($\chi^2_\nu = 0.93$ for 121 dof). Thus the X-ray emission is classified as non-thermal. The emission turns out to be highly absorbed, with $N_H = (2.8 - 3.6) \times 10^{22} \text{ cm}^{-2}$, prohibiting any measurement of the softer cooling emission from the neutron star surface. Figure 3 shows the energy spectrum as observed by the EPIC MOS1/2. The X-ray flux in the 0.5–10 keV band is $f_x = (4.9 - 5.4) \times 10^{-12} \text{ erg s}^{-1} \text{ cm}^{-2}$, implying a luminosity of $L_x = (2.1 - 2.3) \times 10^{34} \text{ erg s}^{-1}$ for a distance of $d = 6$ kpc. The inferred X-ray conversion efficiency is $L_x/\dot{E} = 1.4 \times 10^{-3}$ and 3.6×10^{-4} in the 0.5 – 10 keV and 0.1 – 2.4 keV band, respectively.

Diffuse X-ray emission associated with PSR J1617–5055, either because of the presence of a plerion or a supernova remnant, has not been detected in the XMM-Newton data (cf. Fig.9). Chandra observed PSR J1617–5055 in September 1999 and February 2000. We analyzed the public archive data, and found no indication of diffuse extended emission surrounding PSR J1617–5055 either (Becker et al., 2002a).

In order to investigate the pulsar’s temporal X-ray emission properties we used the data from the EPIC-PN camera which was operated in timing mode with a temporal resolution of 0.03 ms (cf. Tab.1). The presence of the nearby RCW 103 supernova remnant required a tight roll-angle constraint of $268^\circ - 270^\circ$ for the lower and upper position angles in order to minimize source confusion with photons being recorded along the read-out direction of the CCD columns in which PSR J1617 – 5055 was placed. To extract the pulsar events we selected an area of 8×199 pixels from the central CCD #4 of the PN camera. According to the fractional encircled energy function this means that we sample about 70% of the source photons in x - and 100% in y -direction. After barycentrication (we used the source position RA=16:17:29.45, DEC=-50:55:13.61) and correcting for the satellite orbit we searched for the pulsar period using an fft-based algorithm. To optimize the pulsar signal we blocked off all emission below 2.5 keV as the DC level at these energies is found to exceed the pulsar signal due to the emission from the nearby RCW

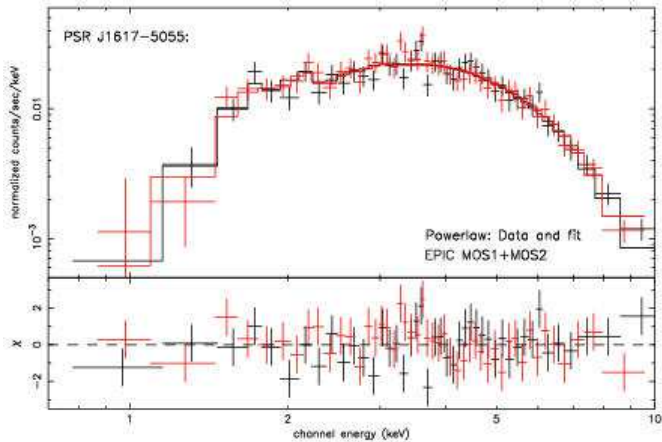


Fig. 3. X-ray spectrum of PSR J1617-5055 taken with MOS1/2 and fit by a power-law.

103, which reduced the signal-to-noise ratio and the detectability of the X-ray pulses significantly. But still with the remaining events we detected strong pulsed emission up to 15 keV. The pulse profile shows a single peak with a duty cycle of $\sim 50\%$ and it shows a pronounced similarity with the radio profile at 1.4 GHz reported by Kaspi et al. (1998). This suggests a close correlation between the radio and X-ray emission mechanisms (cf. Fig.4). Comparing the X-ray pulse profile of PSR J1617-5055 with those observed from other young pulsars we find a striking similarity with PSR 1509-58 and PSR 0540-69. For the epoch MJD=52155.5992851784, which is the mean epoch of the XMM observation in TDB at the solar system barycenter, we measure a period of $P = 69.37252615720$ ms. The accuracy of the XMM clock against UTC is good enough to measure the arrival time of the X-ray pulse which we find at phase 0.65 (center of mass of the pulse) for the epoch given above.

In order to investigate the energy dependence of the X-ray pulse we performed a timing analysis separately for the 2.5 – 4.5 keV, 4.5 – 9.0 keV and 9.0 – 15 keV bands. Neither the overall shape of the pulse nor its phase is found to change with energy. The pulsed fraction we measured in the different energy bands using a bootstrap method (Swanepoel et al. 1996) is $48 \pm 4\%$, $57 \pm 4\%$ and $69 \pm 19\%$ in the 2.5 – 4.5 keV, 4.5 – 9.0 keV and 9.0 – 15 keV bands, respectively. The fraction of the pulsed flux in the 2.5 – 15 keV band is $53 \pm 3\%$.

3.2. Radio-silent Neutron Stars in Supernova Remnants

A fascinating result reflecting the advantage of wide-field spectro-imaging observations provided by ROSAT in its all-sky survey (RASS) is the discovery of the supernova remnant RX J0852.0-4622 by Aschenbach (1998). The remnant is located along the line of sight towards the south-east corner of the Vela supernova remnant (cf. Fig.5). Because the Vela SNR dominates the emission

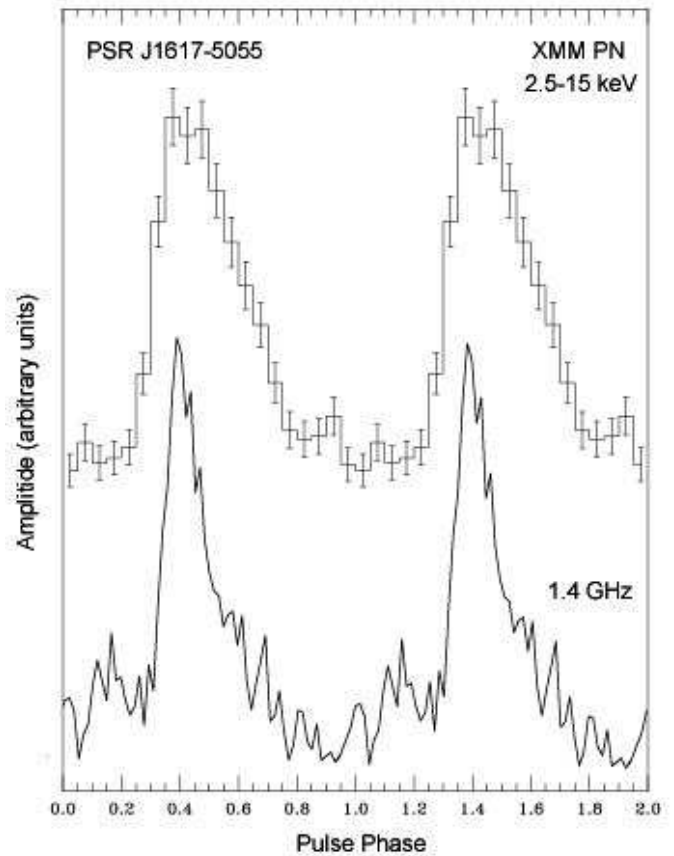


Fig. 4. X-ray and radio pulse profiles of PSR J1617-5055 as observed in the 2.5–15 keV band with the XMM EPIC-PN and at 1.4 GHz with the Parkes Radio Telescope. Both the X-ray and the radio profile show a single peak. The X-ray pulse has a duty cycle of $\sim 50\%$ in the 2.5-15 keV band. Two pulsation cycles are shown for clarity. (The radio pulse profile has been adopted from Kaspi et al. 1998)

in the soft band, RX J0852.0-4622 is best visible in the RASS data at energies above ~ 1 keV. The remnant has a circular shell-like shape with a diameter of 2 degrees. Although the distance to the remnant is quite uncertain, its free-expansion age ($t \sim 3.4 \times 10^3 v_{5k}^{-1} d_{1kpc} \text{ yr}$, with v_{5k} as expansion velocity in units of 5000 km/s) suggests a remnant age much younger than that of Vela. RX J0852.0-4622, often denoted as *Vela-Junior* because of its young age, turns out to be remarkable in several aspects. COMPTEL data suggest that the remnant has a 1.157 MeV γ -line from the radioactive isotope ^{44}Ti exclusively produced in supernovae (Iyudin et al. 1998). If true, the remnant could be as young as ~ 620 years and as close as ~ 200 pc (Aschenbach et al. 1999), making it the closest and youngest supernova remnant among the ~ 250 remnants known today (Green 2000). However, as the detection of the ^{44}Ti line is of low significance, it leaves the age and distance estimates of the remnant widely unconstrained, but see Aschenbach et al. (1999) for a detailed discussion. ASCA observations have shown that

Characteristics of the optical, X-ray and gamma-ray detected rotation-powered field pulsars.

Pulsar	Comment	detected						$\dot{E}/(4\pi d^2)$	$\log \dot{E}$	$\log L_x^{tot}$	$\log L_x^{puls}$	$\log L_x^{pn}$	$\log L_{bol}^\infty$	$\log (P/2\dot{P})$	P	$\dot{P} \times 10^{-15}$	d	$\log B_\perp$
		R	O	X _s	X _h	γ_s	γ_h	erg/s/cm ²	erg/s	erg/s	erg/s	erg/s	erg/s	years	ms	s s ⁻¹	kpc	Gauss
B0531 + 21	Crab	p	p	p	p	p	$9.3 \cdot 10^{-7}$	38.65	35.98	35.85	37.3	≤ 34.1	3.10	33.40	420.96	2.00	12.58	
B0833 - 45	Vela	p	p	p	p	p	$2.3 \cdot 10^{-7}$	36.84	32.25	31.25	32.95	~ 32.3	4.05	89.29	124.68	0.30	12.53	
J0205 + 6449	in 3C58	-	-	p	-	-	$3.2 \cdot 10^{-8}$	37.42	32.20		34.31		3.73	65.67	193.52	2.60	12.55	
J2229 + 6114	in G106.6+2.9	p	-	p	-	d	$2.0 \cdot 10^{-8}$	37.34	33.01				4.02	51.62	78.27	≥ 3	12.30	
J1617 - 5055	near RCW 103	p	-	p	-	-	$1.3 \cdot 10^{-8}$	37.20	33.76	33.48			3.91	69.33	136.05	3.30	12.49	
B0633 + 17	Geminga	p	p	p	-	p	$1.1 \cdot 10^{-8}$	34.51	31.10	30.62		31.2	5.53	237.09	10.97	0.16	12.21	
B1706 - 44	in G343.1-02.3	p	-	p	-	p	$8.6 \cdot 10^{-9}$	36.53	33.15			≤ 33.5	4.24	102.45	93.04	1.82	12.49	
B1509 - 58	in MSH 15-52	p	-	p	p	p	$7.7 \cdot 10^{-9}$	37.25	34.29	34.10	35.3	≤ 33.9	3.19	150.23	1540.19	4.30	13.19	
B1951 + 32	in CTB 80	p	-	d	-	p	$5.0 \cdot 10^{-9}$	36.57	33.44		34.0	≤ 33.9	5.03	39.53	5.85	2.50	11.69	
J1930 + 1852	in G54.1+0.3	p	-	p	-	-	$4.0 \cdot 10^{-9}$	37.08					3.46	136.85	750.20	~ 5	13.00	
J1811 - 1926	in G11.2-0.3	-	-	p	-	-	$2.4 \cdot 10^{-9}$	36.80					4.38	64.67	44.00	≥ 5	12.23	
B1046 - 58	Vela twin	p	-	d	-	p	$1.9 \cdot 10^{-9}$	36.30	≤ 32.11			≤ 32.7	4.31	123.65	95.92	2.98	12.54	
B1259 - 63*	Be-star/bin	p	-	d	d	d	$1.7 \cdot 10^{-9}$	35.92	32.95			≤ 33.8	5.52	47.76	2.27	2.00	11.51	
J0537 - 6909	in N157B/LMC	p	-	p	-	-	$1.6 \cdot 10^{-9}$	38.68					3.71	16.11	51.24	49.4	11.96	
J1420 - 6048		p	-	p	-	-	$1.4 \cdot 10^{-9}$	37.00	34.46				4.11	68.18	82.85	7.70	12.38	
B1823 - 13	Vela like	p	-	d	-	-	$1.4 \cdot 10^{-9}$	36.45	33.39			≤ 33.9	4.33	101.45	74.95	4.12	12.45	
B1800 - 21	G8.7-0.1	p	-	d	-	-	$1.2 \cdot 10^{-9}$	36.35	33.06			≤ 33.8	4.30	133.61	134.32	3.94	12.63	
B1929 + 10		p	d	p	-	-	$1.1 \cdot 10^{-9}$	33.59	30.00	29.5		≤ 31.4	6.49	226.51	1.16	0.17	11.71	
B0656 + 14	cooling NS	p	p	p	-	?	$5.5 \cdot 10^{-10}$	34.58	32.98	32.15		32.9	5.05	384.87	55.03	0.76	12.67	
B0540 - 69	in N158A,LMC	p	p	p	p	-	$5.1 \cdot 10^{-10}$	38.17	36.21	36.1	37.2	≤ 36.1	3.22	50.37	479.06	49.4	12.70	
J1105 - 6107		p	-	d	-	-	$4.3 \cdot 10^{-10}$	36.40					4.80	63.19	15.80	7.00	12.00	
B0950 + 08		p	?	d	-	-	$3.3 \cdot 10^{-10}$	32.75	29.35			≤ 31.0	7.24	253.06	0.23	0.12	11.39	
B1610 - 50		p	-	d	-	-	$2.5 \cdot 10^{-10}$	36.20					3.87	231.60	492.54	7.26	13.03	
J0538 + 2817	in G180.0-1.7	p	-	d	-	-	$1.3 \cdot 10^{-10}$	34.69	32.74			≤ 33.6	5.79	143.15	3.66	1.50	11.87	
B1055 - 52	cooling NS	p	d	p	-	p	$1.1 \cdot 10^{-10}$	34.48	33.42	32.57		33.5	5.73	197.10	5.83	1.53	12.03	
B0355 + 54		p	-	d	-	-	$8.8 \cdot 10^{-11}$	34.66	31.96			≤ 33.8	5.75	156.38	4.39	2.07	11.92	
B2334 + 61	G114.3+0.3	p	-	d	-	-	$8.6 \cdot 10^{-11}$	34.79	31.86			≤ 33.4	4.61	495.24	191.91	2.46	12.99	
B0823 + 26		p	-	d	-	-	$2.6 \cdot 10^{-11}$	32.66	29.83			≤ 31.0	6.69	530.66	1.72	0.38	11.99	

Table 3. List of rotation-powered pulsars that have been detected in the radio, optical, X- and/or γ -ray wavebands, ordered according to their spin-down flux density at Earth $\dot{E}/4\pi d^2$. The individual columns are as follows: 1. Pulsar name; 3-8. Energy ranges in which pulsed (p), unpulsed (d) radiation has been detected: R - radio, O - optical, X_s - soft X-rays ($E_\gamma \sim 1\text{keV}$), X_h - hard X-rays ($E_\gamma \sim 10\text{keV}$), γ_s - soft γ -rays ($E_\gamma \sim 1\text{MeV}$) and γ_h - hard γ -rays ($E_\gamma > 100\text{MeV}$). Possible detections are indicated by a question mark. \dot{E} is the pulsar spin-down power $I\dot{\Omega}\dot{\Omega}$; $L_x^{tot} = 4\pi d^2 f_x$ is the sum of the pulsed and unpulsed X-ray luminosity. L_x^{puls} is the pulsed luminosity; L_x^{pn} is the total X-ray luminosity including synchrotron nebula emission. All luminosities L_x are calculated for the ROSAT energy range 0.1 - 2.4 keV. For Geminga, PSR 0656+14 and 1055-52 thermal and non-thermal contributions are included. L_{bol}^∞ is the bolometric luminosity. The upper limits have been computed for a neutron star with a medium stiff equation of state (FP-Model, $M = 1.4 M_\odot$ and $R = 10.85$ km). *PSR 1259-63 was observed $\sim 13^\circ$ post-apastron. For references see Becker & Trümper (1997; 1999) and Becker & Pavlov (2002) and references therein. Radio pulsar parameters have been taken from Manchester et al. (2002). A summary of the optical and γ -ray observations can be found in Caraveo et al. (2002) and Kanbach (2002, this proceedings).

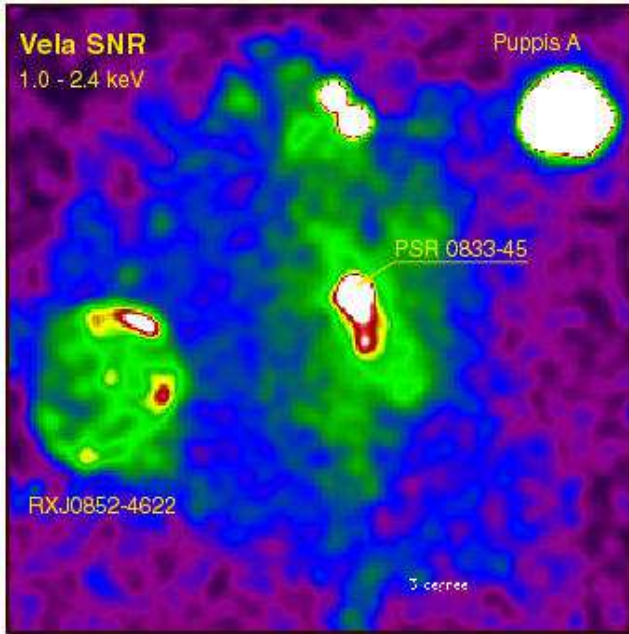


Fig. 5. Vela and friends: The two supernova remnants Puppis A and RX J0852.0-4622 are both located at the edge of the Vela supernova remnant. Emission from the neutron star CXOU J085201.4-461753 is clearly visible in the ROSAT all-sky survey image near to the center of RX J0852.0-4622.

the X-ray emission of the brightest parts of the remnant are dominated by non-thermal emission (Tsunemi et al. 2000; Slane et al. 2001) with a column density about one order of magnitude larger than what is known for the Vela supernova remnant. Together with SN1006 and G347.3-0.5, RX J0852.0-4622 thus form the first members of the exclusive group of non-thermal shell-type supernova remnants, believed to be accelerators of cosmic rays. The lack of strong variation in N_H across RX J0852.0-4622 further indicates that the remnant cannot be more distant than the Vela Molecular Ridge (Slane et al. 2001), locating it most likely behind the Vela remnant at a distance between 1-2 kpc.

The remnant and its emission properties are interesting by its own and justify deep and detailed X-ray studies, but a compact central X-ray source has been detected in the remnant as well. First recognized as a 5σ excess in the RASS data by Aschenbach et al. (1998) its existence was supported by the detection of a hard, somewhat extended X-ray source in the ASCA data (Tsunemi et al. 2000; Slane et al. 2001). To conclusively identify this source as the compact remnant of the supernova explosion that created RX J0852.0-4622 was not possible because of the presence of two foreground stars (HD 76060 and Wray 16-30) which could be responsible for at least part of the central X-ray emission. But a recent observation with the Chandra ACIS-I has clearly invalidated the association with either one of these stars (Pavlov et al. 2001) and another faint but hard X-ray source found

by Mereghetti (2001) in a recent BSAX observation. In view of this, there is little doubt that the central X-ray source CXOU J085201.4-461753, located only 4 arcmin off the geometrical center of RX J0852.0-4622, indeed is the compact remnant of the supernova explosion. This is further supported by the f_x/f_{opt} ratio as the source has no optical counterpart brighter than $m_B \sim 22.5$. The short 3 ksec Chandra observation provides only an accurate position for CXOU J085201.4-461753. Spectral analysis is strongly hampered by small photon statistics and pile-up effects (Pavlov et al. 2001). There is no extended X-ray emission reported from this short Chandra observation.

The central part of RX J0852.0-4622 was observed on 2001 April 27 by XMM-Newton in the course of the guaranteed time program (Becker et al. 2002a). The exposure time was ~ 25 ksec. In all observations, the MOS1/2 and the PN cameras were operated in full-frame and extended full-frame mode, respectively. An image of the central part of RX J0852.0-4622 as seen with the MOS1/2 is displayed in Fig.6. CXOU J085201.4-461753 is the brightest source in the field. It is located at the western edge of a faint diffuse and irregularly shaped X-ray structure. The extended emission was already visible in ASCA images, but less resolved from the neutron star because of ASCA's wider point spread function. As the whole remnant emits non-thermal X-ray emission along with a small thermal contribution from the Vela remnant, it was not possible to conclusively identify the extended structure in the ASCA images as plerionic (Slane et al. 2001). The XMM-Newton observation thus allowed for the first time a somewhat more detailed view of the field. The extended source has a size of $\sim 9' \times 14'$ and emits mostly in the soft band below ~ 2 keV. A MOS1/2 image showing the field in the 2.0-12 keV band is displayed in Fig.7. No significant emission from the extended structure is visible beyond ~ 2 keV.

Fitting model spectra to the data from CXOU J085201.4-461753, we tested the usual blackbody and power-law models as well as models consisting of two blackbody components and a blackbody and power-law component, respectively. With a reduced χ^2 of 0.952 (for 218 dof) the single blackbody model provides an excellent fit to the data, implying a column density of $N_H = (3.7 - 4.3) \times 10^{21} \text{cm}^{-2}$, a temperature in the range $(4.28 - 4.50) \times 10^6$ K and a formal emitting area of $R_{bb} = (0.31 - 0.36)$ km for an assumed distance of 1 kpc. The unabsorbed X-ray flux and luminosity are $f_x = (1.82 - 2.96) \times 10^{-12} \text{erg cm}^{-2} \text{s}^{-1}$ and $L_x(d=1 \text{ kpc}) = (2.17 - 3.53) \times 10^{32} \text{erg s}^{-1}$ in the 0.5 - 10 keV band, respectively. All parameters are given for a 90% confidence range. Compared with the blackbody fit, the power-law model is invalidated by a larger reduced χ^2 of 1.21 and residuals which indicate systematic deviations from the measured data points. The fitted photon index of $\alpha = 4.38 - 4.62$ is much steeper than what is usually found in other young neutron stars which are well known for their non-thermal emission. The blackbody fit, how-

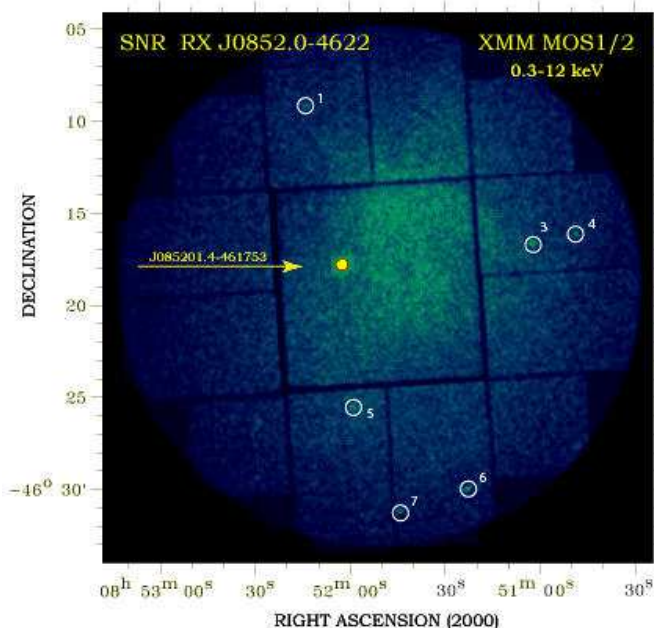


Fig. 6. XMM’s view of the ~ 30 arcmin diameter part centered on RX J0852.0-4622. Data from MOS1 and MOS2 have been merged to produce the image. A few other faint and point-like sources, indicated by circles, are detected in the field of view.

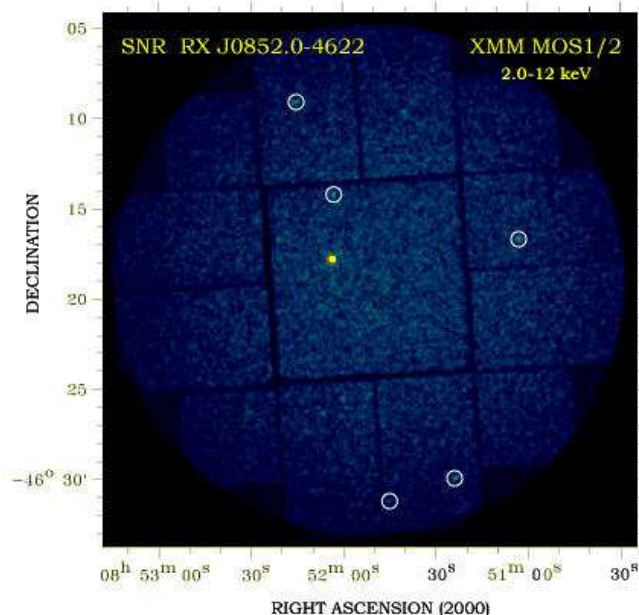


Fig. 7. The central part of RX J0852.0-4622 in the energy band 2.0 – 12 keV. Only very faint residual emission from the extended structure surrounding CXOU J085201.4-461753 is visible.

ever, indicates a small unmodeled emission in the hard band beyond ~ 3 keV. We therefore tested a compound model consisting of a blackbody and an additional power-law component and fitted the non-thermal spectrum with

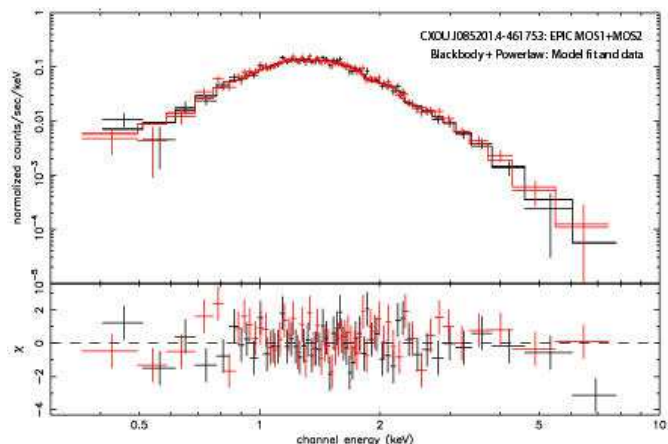


Fig. 8. The spectrum of CXOU J085201.4-461753 obtained with XMM MOS1/2 and fitted with a blackbody plus power-law model. The residuals of the fit are shown.

a photon index of $\alpha = 2.85 \pm 1.5$. The flux and luminosity of these component are $f_x = 3.7 \times 10^{-13} \text{ erg s}^{-1} \text{ cm}^{-2}$ and $L_x(d=1 \text{ kpc}) = 4.4 \times 10^{31} \text{ erg/s}$.

The temperature along with the small size of the emitting region invalidates the interpretation that the thermal radiation is emission from cooling of the entire neutron star surface. If the blackbody model is the right description it points towards emission from a hot polar cap region on the neutron star surface. In the literature various models have been proposed to produce hot spots on the neutron star surface. Almost all magnetospheric emission models predict a bombardment of the polar cap regions by energetic particles accelerated in the magnetosphere backwards to the neutron star surface (cf. Cheng, Ho & Ruderman 1982; Harding & Muslimov 2002 and references therein). Though CXOU J085201.4-461753 is not known to be a radio pulsar it still could be possible that the hot polar caps are heated by particle bombardment while the radio emission itself is undetected due to an unfavorable beaming geometry. This is not an unlikely scenario. The opening angle of a radio beam is inversely proportional to the square root of the pulsar’s rotation period so that the radio beams of slowly rotating pulsars can easily miss the observers line of sight and thus keep undetected.

The heat transport in neutron stars is accomplished by electrons and positrons. A strong magnetic field is therefore expected to have an essential impact on the neutron star cooling as it channels the heat transport along the magnetic field lines and suppresses it in the perpendicular direction. Neutron star cooling with a full treatment of a strong magnetic field thus should lead to an anisotropic heat flow and subsequently to an anisotropic surface temperature distribution, with the polar cap regions hotter than the equatorial regions.

A great advantage of the CCD based EPIC detectors aboard XMM is that they not only provide spatial and high resolution spectral information but have observing

modes which are fast enough for timing studies even of millisecond pulsars (Becker et al. 2002; Kuster et al. 2002; Kendziorra et al. 2002). During the observation of CXOU J085201.4-461753 the MOS1/2 and PN cameras were operated in full frame and extended full frame mode, providing a temporal resolution of 2.6 s and 200 ms, respectively. While this is not fast enough to search for coherent pulsations on a millisecond time scale, it allows to search the signal for periodicities in a period range in which anomalous X-ray pulsars (AXPs) are seen. Application of fft-based search algorithms along with a more detailed periodicity search around possible frequency candidates, however, did not result in a detection of a significant periodic signal.

Another example of a radio silent neutron star in a supernova remnant is 1E 161348–5055, the projected location of which is in RCW 103 (cf. Fig.9). This source was discovered with the Einstein Observatory (Tuohy & Garmire 1980) and has an estimated age of ~ 2000 yrs. The remnant is mostly known for its central point source, which was considered for many years to be the prototype of a cooling neutron star. No X-ray pulsations and no radio or optical counter part could be detected. ROSAT observations suggested that the source emits hard X-rays (Becker et al. 1993). Comparing two ASCA observations of RCW 103 Gotthelf, Petre & Vasisht (1999) found an order-of-magnitude decrease in luminosity over four years, which suggests that this object may be an accreting source rather than a cooling neutron star. Likewise puzzling is the ~ 6 h periodicity of its flux reported by Garmire et al. (2000) from Chandra observations and archival ASCA data.

XMM has observed RCW 103 in September 2001 for an exposure time of 20 ksec. Figure 9 shows a false color image of the remnant, derived from the XMM MOS1/2 data. These data provide for the first time detailed spectral information on the central point source. Chandra has observed the remnant in September 1999 and February 2001. Albeit superior imaging, small counting statistics in the first observation and severe pile-up effects in the second observation preclude a meaningful spectral analysis. The energy spectrum of 1E 161348–5055 extracted from XMM MOS1/2 data is shown in Fig. 10. The status of the detector response matrix which is available for the EPIC-PN small-window mode and which is still preliminary, did not allow to include this data in the analysis up to now, but will provide additional spectral information in the 0.3 – 10 keV band. Fitting various spectral models to the MOS data a simple blackbody was found to describe the data almost up to ~ 5 keV, but leaving unmodeled hard emission beyond. A single power-law fit is acceptable on statistical grounds but requires a photon spectral index of 4.1 – 4.2. Testing two component models, a double blackbody is found to describe the data best ($\chi^2_{\nu} = 1.0$ for 287 dof), resulting in $N_H = (1.5 - 1.8) \times 10^{22} \text{ cm}^{-2}$, temperatures of $T_1 = (4.1 - 5.1) \times 10^6 \text{ K}$ and $T_2 = (8.3 - 10) \times 10^6 \text{ K}$ with $R_1^{bb} = 1.7 - 3 \text{ km}$ and $R_2^{bb} = 220 - 500 \text{ m}$ for the blackbody radii of the emitting areas (assuming a distance

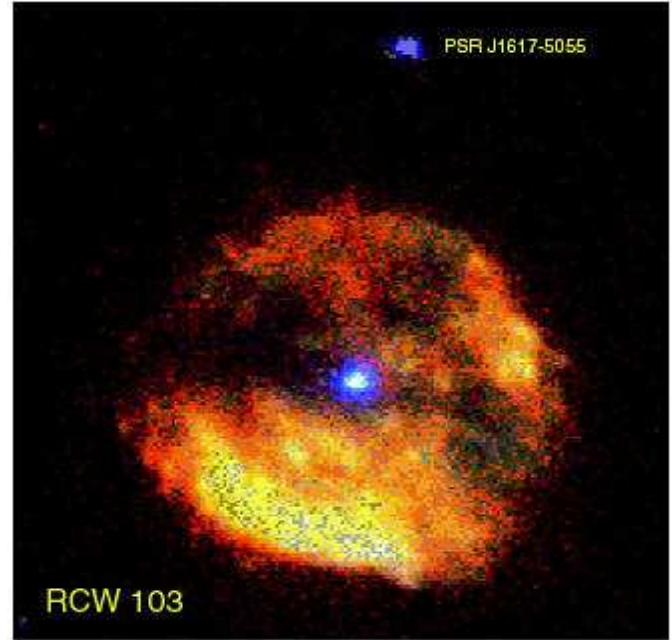


Fig. 9. XMM MOS1/2 image of the supernova remnant RCW 103. The red color represents photons in the 0.3 – 0.75 keV band, green and blue correspond to $\sim 0.75 - 2$ keV and $2 - 10$ keV, respectively. The neutron star candidate is the hardest X-ray source in the remnant. The 69 ms pulsar PSR J1617–5055 is located 7 arcmin off the supernova center. The remnant extent is $\sim 10'$.

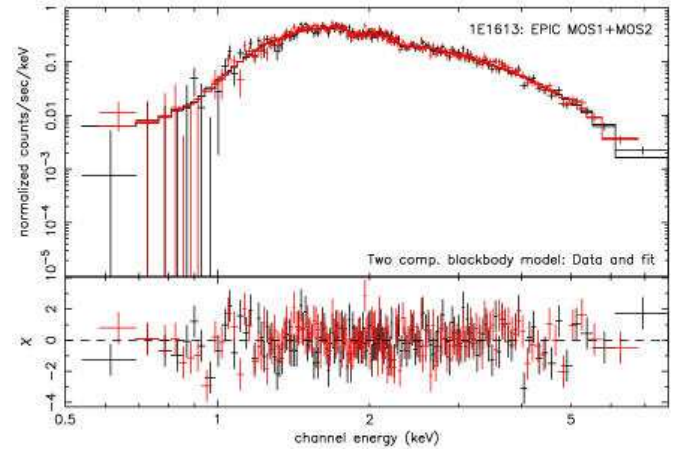


Fig. 10. X-ray spectrum of 1E 161348–5055 in RCW 103 obtained from XMM MOS1/2 data. The spectrum is fitted by a two component blackbody model. Red and black data points are from the MOS1 and MOS2 cameras, respectively. A small spectral feature is seen at ~ 0.98 keV.

of $d = 3.3$ kpc). The given numbers represent the 90% confidence range. This result suggests that the first thermal component is emitted from a rather large fraction of the surface, whereas the second component requires a much smaller emitting area like a polar cap region. Compared with the surface temperatures predicted by neutron star

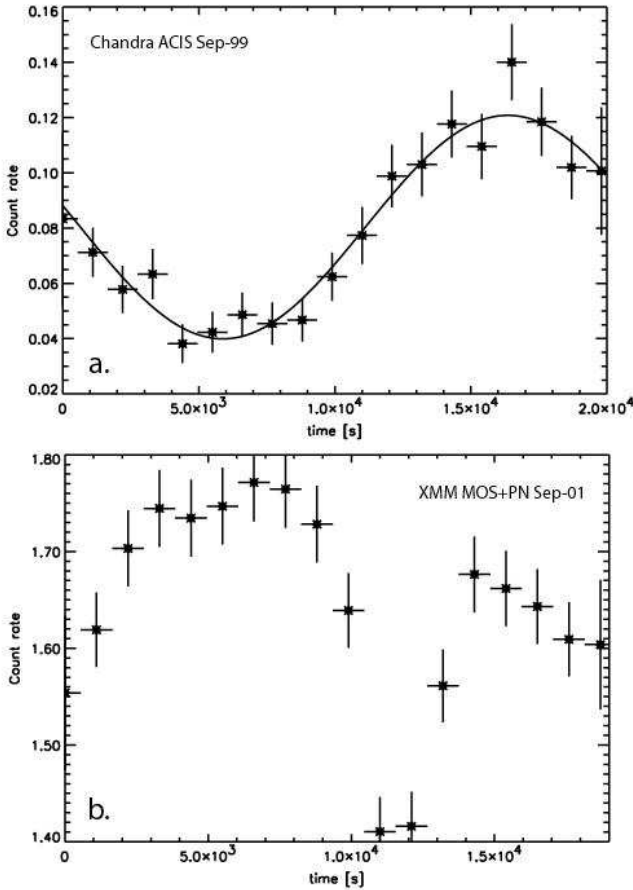


Fig. 11. X-ray lightcurve of 1E 161348–5055 observed with Chandra (a.) and XMM-Newton (b.) in September 1999 and 2001, respectively. The Chandra lightcurve indicates a sinusoidal modulation with a period of ~ 6 h. The lightcurve observed by XMM-Newton shows for the first time clear indication of an eclipse and thus identifies 1E 161348–5055 as a neutron star in a binary system (Becker 2001).

cooling models, T_1 is much higher than what is expected for a ~ 2000 yr young neutron star.

In addition to the long term flux change the Chandra data suggested a ~ 6 h periodicity. Archival ASCA data were found to be consistent with this. However, a second Chandra observation taken in Feb 2000 did not really confirm this periodicity and was more consistent with a ~ 4 h period, although 1E 161348–5055 was about ten times brighter at that time than in September 1999. It was therefore of special interest to see the lightcurve of 1E 161348–5055 taken with XMM-Newton in September 2001. Figure 11 shows the lightcurve taken with Chandra and XMM-Newton in September 1999 and 2001, respectively. The lightcurve taken by XMM-Newton does not show the ~ 6 h periodicity but discovers an eclipse about 3h after the start of the observation, identifying 1E 161348–5055 as the second accreting binary in a supernova remnant. The companion most likely is a low-mass

companion. Chandra observations taken in March 2002 confirm the XMM findings (Sanwal et al., 2002). The discovery of a candidate optical counterpart in the near-IR was reported by Pavlov et al. (these proceedings).

Similar to the previous examples is the point source RX J0822–4300 in Puppis-A (cf. Fig.5). With a distance of about 2.2 kpc the remnant is further away than the Vela supernova remnant. The kinematic age is estimated to $\sim 3500 - 4000$ years, and is therefore a factor of about three younger than the Vela SNR. Discovered in Einstein data, it became evident with ROSAT that RX J0822–4300 is most likely the neutron star expected to form in the SN event (Petre, Becker & Winkler 1996). As for CXOU J085201.4-461753 there is no radio emission detected from this source down to 0.75 mJy and no optical counterpart could be detected down to an observation limit of about 24 mag.

In order to study the nature of RX J0822-4300 in greater detail, the central part of Puppis-A was observed by XMM-Newton in April and December 2001 for 20 kec and 30 ksec, respectively. Figure 12 shows the false color image of the central part of the remnant taken with the two MOS1/2 cameras in April 2001. Like in RCW 103, the neutron star candidate is the hardest X-ray source in the remnant.

The analysis of the RX J0822–4300 emission reveals an X-ray spectrum similar to that observed for 1E 161348–5055. Fitting the data with a simple blackbody model doesn't describe the spectrum beyond ~ 3 keV. A two component blackbody model and a model consisting of a blackbody and a power-law are fitting the spectrum equally well. The double blackbody spectrum yields $N_H = (3.6 - 4.4) \times 10^{21} \text{ cm}^{-2}$, temperatures of $T_1 = (3.4 - 4) \times 10^6$ K and $T_2 = (0.6 - 1.3) \times 10^7$ K with $R_1^{bb} = 1.4 - 1.8$ km and $R_2^{bb} = 40 - 310$ m for the blackbody radii of the corresponding emitting areas (assuming a distance of $d = 2.2$ kpc). A model consisting of a blackbody and a power-law yields similar results for the dominating blackbody component ($N_H = (2.9 - 3.6) \times 10^{21} \text{ cm}^{-2}$, $T = (4.3 - 4.5) \times 10^6$ K, $R^{bb} = 1.1 - 1.3$ km) but fits the hard emission with a power-law of photon-index $\alpha = 2.0 - 2.7$ (90% confidence). This slope is in agreement with what is observed for other young pulsars showing magnetospheric emission.

Zavlin et al. (1999) have modeled the ROSAT data of RX J0822–4300 including a hydrogen atmosphere on top of the neutron star. These models reduce the temperature of the thermal component by a factor of ~ 2 and require a somewhat larger size for the emitting region. Spectral fits which take into account models of a non-magnetic neutron star atmosphere of pure H or He are currently in progress. The X-ray luminosities based on the two component models are in the range $L_x = (3 - 4) \times 10^{33} \text{ erg/s}$.

The EPIC-PN camera observed RX J0822–4300 in small-window mode restricting the field of view to $4' \times 4'$ but with a time resolution of 6 ms. Using archival ROSAT data of RX J0822–4300 Zavlin et al. (1999) found evi-

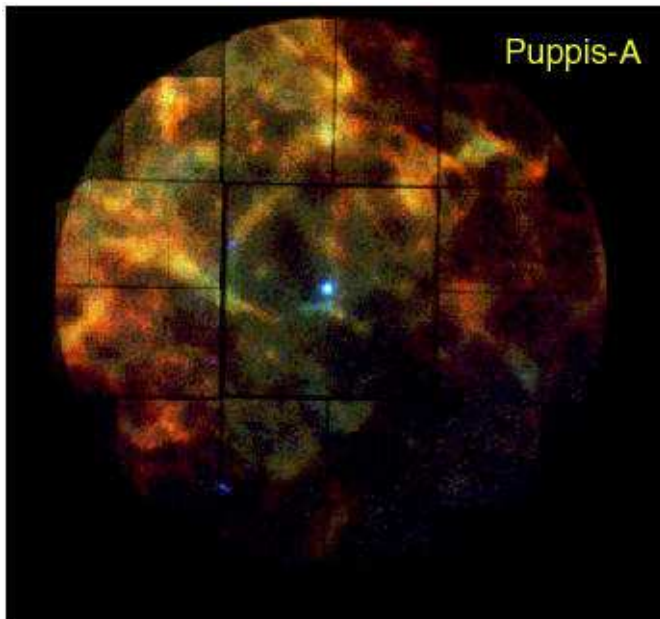


Fig. 12. False color image of the central part of Puppis-A, depicting an area of 15 arcmin in radius centered on RX J0822–4300. The red color represents photons which are detected in the 0.3 – 0.75 keV band, green and blue correspond to $\sim 0.75 - 2$ keV and $2 - 10$ keV, respectively. Note the amazing honeycomb structure seen in the remnant emission.

dence for X-ray pulsations with a period of ~ 75.3 ms. The XMM-Newton data, however, which are of much better statistical quality than the ROSAT data do not confirm this periodicity, leaving the rotation period of the neutron star candidate unknown.

From the observations of radio-silent compact objects in supernova remnants one can conclude that the emission properties of such sources are quite different compared to ordinary radio pulsars. On the other hand, it is very plausible that they are more common than radio pulsars, and the relatively small number of the members of this class discovered so far is mainly due to observational selection effects. It is much easier to detect and identify active radio or X-ray pulsars than these “radio-quiet” sources observable only in the X-ray band and located in a patchy X-ray bright supernova remnant environment.

4. The cooling neutron stars

As discussed in §2, soft X-ray radiation of rotation-powered pulsars of an age between $\sim 10^5 - 10^6$ yrs should be dominated by emission from the cooling hot neutron star surface. These pulsars are old enough for their magnetospheric emission to become fainter than the thermal surface emission, but they are still young and hot enough to be detectable in the soft X-ray range. There are three middle-aged pulsars, i.e. Geminga, PSR B0656+14 and B1055–52, from which thermal X-ray radiation from the surface of the cooling neutron star has

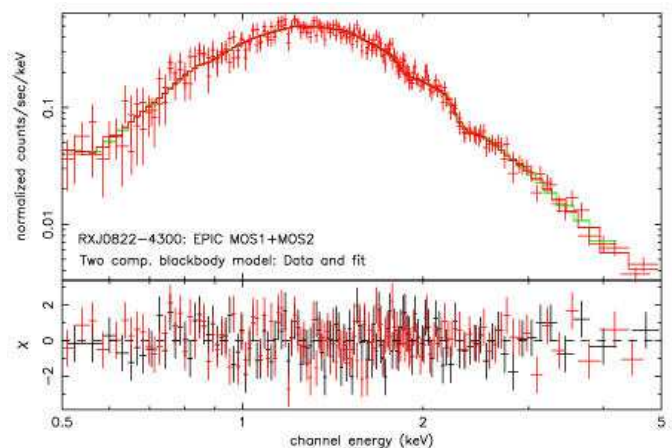


Fig. 13. X-ray spectrum of the point source RX J0822–4300 in Puppis-A derived from XMM MOS1/2 data. The spectrum is fitted by a two component blackbody model. Red and black data points represent the data taken with the MOS1 and MOS2 cameras, respectively. The residuals of the fits shown below amount to a reduced χ^2_ν value of 0.9444 for $\nu = 244$ degrees of freedom.

certainly been observed. Because of the similarity of their emission properties, they were dubbed as *the three Musketeers* by Becker & Trümper (1997). It follows from the ROSAT and ASCA observations of the brightest middle-aged pulsar B0656+14 that the thermal component cannot be described by a single temperature blackbody spectrum, i.e. the neutron star surface temperature is not uniform (Greiveldinger et al. 1996). In a simple model the thermal component consists of a soft thermal component (TS) from most of the neutron star surface (at $E \lesssim 0.5 - 1$ keV) and a hard thermal component (TH) from hot polar caps, heated by relativistic particles, for instance. Alternatively, the temperature non-uniformity can be due to an anisotropic heat conductivity in the neutron star crust caused by the anisotropic magnetic field — the heat flux across the field is reduced whereas it is preferred in directions perpendicular to the field, so that the magnetic poles are expected to be hotter than the equatorial regions (Potekhin & Yakovlev 2001). The thermal component dominates in the UV through the soft X-ray range (up to 1 – 2 keV), whereas the non-thermal component described by a power-law (PL) spectrum prevails in the IR, optical, hard X-ray and gamma-ray bands.

PSR 1055-52 and Geminga are not as luminous as PSR 0656+14. Their spectra measured by ROSAT and/or ASCA are well described by a two component model consisting of a blackbody (TS) and a non-thermal (PL) component. Whether a second thermal spectral component (TH) was not detected because of poor counting statistics or whether the component is intrinsically absent has been a pending question which prompted observations with XMM-Newton.

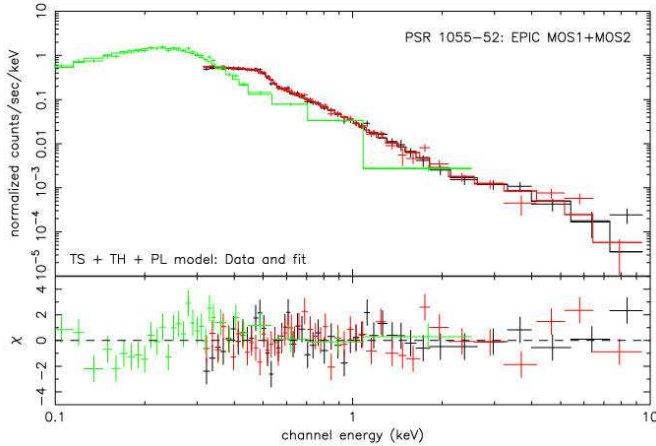


Fig. 14. X-ray spectrum of PSR 1055–52 derived from ROSAT and XMM MOS1/2 data. As for PSR 0656+14 the spectrum requires three components consisting of two thermal (TS+TH) and a harder non-thermal power-law component (PL). The green points represent ROSAT data. Red and black points represent MOS1 and MOS2 data, respectively.

PSR 1055-52 was observed by XMM-Newton for about 96 ksec in December 2000. The X-ray spectrum is shown in Figure 14. It is interesting to note that the two component spectral model which describes the ROSAT and ASCA data does not fit the pulsar spectrum observed by XMM-Newton (Becker 2001). Including the ROSAT data in the spectral analysis, 3 spectral components are required to fit the spectrum in the wide band from 0.1–10 keV. The pulsar’s spectral properties are thus indeed found to match those observed in PSR 0656+14. The soft thermal component (TS) yields a blackbody temperature of $T_{TS} = (7.1 \pm 0.3) \times 10^5$ K, similar to what was obtained from the ROSAT data with a somewhat smaller error, though. The second and harder thermal component (TH) is described by $T_{TH} = (1.4 \pm 0.1) \times 10^6$ K. The corresponding blackbody emitting areas are $R_{TS} = 31 \pm 2$ km and $R_{TH} = 2.6 \pm 0.3$ km, respectively, assuming a distance of 1.5 kpc. The non-thermal component (PL) is described by a power-law with a photon index of $\alpha = 1.89 \pm 0.32$. The column absorption is $N_H = (2.1-2.4) \times 10^{20} \text{ cm}^{-2}$ (all errors represent 90% confidence limits). For the unabsorbed flux in the 0.5–10 keV band we obtain for each of the three components $f_x^{TS} = 2.3 \times 10^{-13} \text{ erg s}^{-1} \text{ cm}^{-2}$, $f_x^{TH} = 2.1 \times 10^{-13} \text{ erg s}^{-1} \text{ cm}^{-2}$ and $f_x^{PL} = 1.4 \times 10^{-13} \text{ erg s}^{-1} \text{ cm}^{-2}$. The corresponding bolometric luminosities are $L_{TS} = 1.74 \times 10^{33} \text{ erg s}^{-1}$ and $L_{TH} = 1.9 \times 10^{32} \text{ erg s}^{-1}$. For the luminosity of the non-thermal component we obtain $L_x = 3.8 \times 10^{31} \text{ erg s}^{-1}$. More detailed results on the pulsar spectrum as well as the results of a phase resolved spectral analysis are given in Becker et al. (2002b).

It should be stressed that the inferred effective temperatures, and hence the radius-to-distance ratios, depend on the model used to describe the thermal component. For

instance, if one assumes that the neutron star surface is covered by a hydrogen or helium atmosphere, the effective temperatures are lower than those derived from the simple blackbody fits by a factor of 1.5 – 3 (Pavlov et al. 1995). Atmospheres dominated by heavy elements give temperatures close to the blackbody temperatures. However, the heavy element atmosphere spectra should show numerous absorption lines and photo-ionization edges (Rajagopal & Romani 1996; Zavlin et al. 1996). Recent observations by Chandra and XMM-Newton of PSR 0656+14 (Marshall & Schulz 2001) as well as of the neutron stars RXJ 1856.5-3754 (Burwitz et al. 2001) and RX J0720.4-3125 (Paerels et al. 2001) have not shown any sign for line emission from a neutron star atmosphere but are perfectly consistent with a pure blackbody like emission.

The X-ray pulses of PSR 1055–52 were discovered by Ögelman & Finley (1993) using ROSAT data. The temporal emission properties were found to indicate a phase shift of about 100° at 0.5 – 0.6 keV accompanied by an apparent increase in the pulsed fraction from $\sim 10\%$ to $\sim 65\%$. Although the narrow bandwidth of ROSAT along with a decreasing sensitivity beyond 1 keV resulted in large errors of the energy dependent pulsed fraction and phase shift, it was suggested that this dichotomy is associated with the thermal and non-thermal emission components seen in the pulsar’s X-ray spectrum. The non-thermal magnetospheric emission is expected to be stronger beamed than the thermal one. Magnetospheric emission thus could show up with a pulsed fraction of up to 100%, depending on the viewing geometry.

XMM-Newton has observed PSR 1055-52 with the EPIC-PN camera set up in timing mode. As described in the introduction (cf. §1), this mode is very sensitive to any enhanced background emission which is accumulated over the whole CCD and condensed along with the source signal into a 1D-image. After barycentering the photon arrival times and correcting for the satellite orbit, the timing signal is detected with high significance. The X-ray pulse profiles, which are shown for different energy bands in Fig.15, are all approximately sinusoidal. A reason for this sinusoidal shape could be the non-uniformity of the surface temperature due to the presence of a strong magnetic field of $\sim 5 \times 10^{12}$ G, as discussed above.

Figure 16a shows the pulsed fraction P_f as a function of photon energy. P_f increases from $\sim 15\%$ in the 0.3–0.4 keV band up to $\sim 80\%$ in the 1.1–1.2 keV band. The fraction of the pulsed flux at higher energies is undetermined in the EPIC-PN data. The observed decrease at $E \geq 1.3$ keV is due to an enhanced background signal, caused by soft proton flares which contaminate the observation and which can not be corrected for. The high background together with a fast decline of the pulsar emission beyond ~ 2 keV causes a strong reduction of the signal-to-noise ratio in the hard energy band, preventing the detection of X-ray pulsations in the EPIC-PN data from most of the non-thermal (PL) emission component. The phase angles

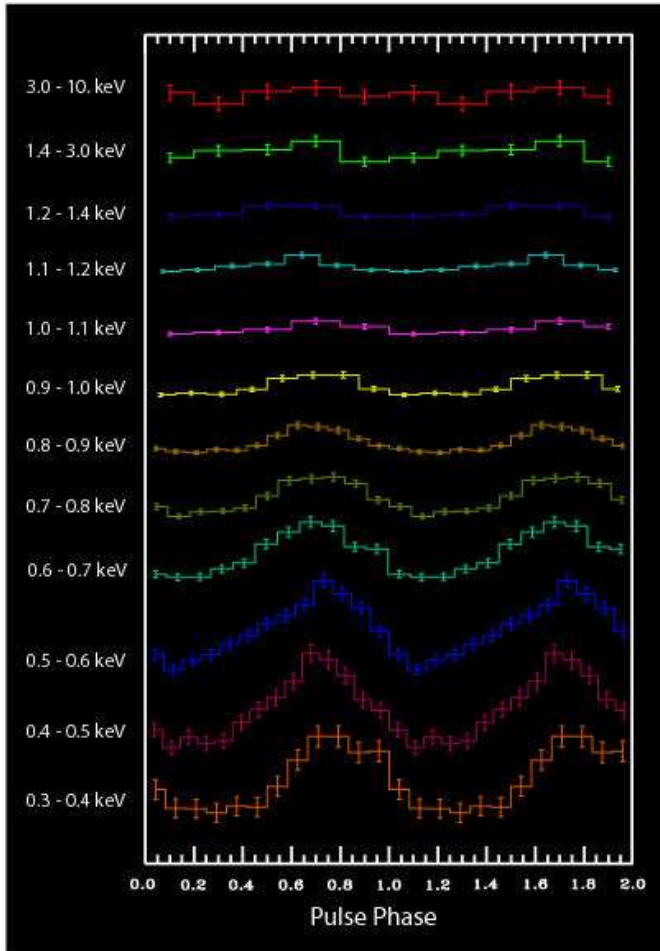


Fig. 15. X-ray pulse profiles of PSR 1055–52 for different energy bands. The pulse profile is sinusoidal. Two complete cycles are shown for clarity. The energy dependent phase shift in the 0.3 – 3 keV band is not as significant as suggested from ROSAT observations.

of the X-ray pulses observed in different energy bands is shown in Figure 16b. The XMM data indicate that the energy dependence of the pulse phase is by far not as strong as indicated by ROSAT. This can also be seen in the pulse profiles shown in Fig. 15.

Since all active pulsars are powerful sources of strong winds, one should expect that they generate pulsar-wind nebulae (PWNe), similar to those observed around the Crab-like and Vela-like pulsars. The PWN sizes should scale as $(\dot{E}/p_0)^{1/2}$, where p_0 is the pressure of the ambient medium. The existence of X-ray bright PWNe (albeit of much larger sizes) around several pulsars, including the three musketeers, was reported by Kawai & Tamura (1996) based on ASCA observations. In addition, the suggestion of a clumpy pulsar-wind nebula near to PSR B1055–52 was made by Shibata et al. (1997). The authors proposed the "clumps" of X-ray emission to be created by the interaction of a pulsar-wind outflow with the local interstellar environment. The very low signal-to-noise ratio

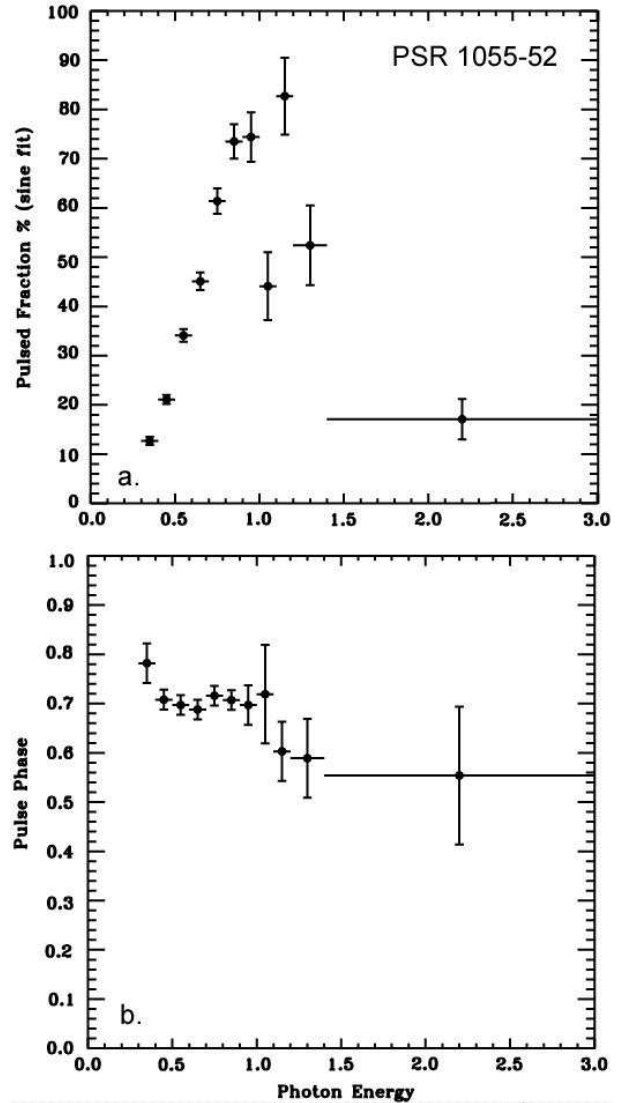


Fig. 16. a. Fraction of pulsed flux vs. photon energy observed for PSR 1055–52 by XMM-Newton. The pulsed fraction peaks at ~ 1.1 keV and decreases beyond that energy. The decrease goes along with a decreasing signal-to-noise ratio which we suggest to be caused by the fading pulsar signal at higher energies in combination with a high DC level from soft-proton flares which are present over the whole observation. Note the dip in the pulsed-fraction at ~ 1 keV. **b.** Pulse phase vs. photon energy. The XMM-Newton data are in agreement with no significant phase shift in the 0.4-3 keV band. A significant pulsed signal is seen up to ~ 3 keV only.

of the "clumps", however, limited any detailed analysis based on just the ASCA data. In an analysis combining BeppoSAX and ROSAT data, Becker et al. (1999) confirmed the existence of X-ray sources surrounding PSR 1055–52 but came to a different conclusion with respect to its interpretation. With ROSAT, and partly with BeppoSAX, the clumpy X-ray emission was resolved as the superposition of a number of point sources, well separated from the pulsar and unlikely to be associated with it. Sev-

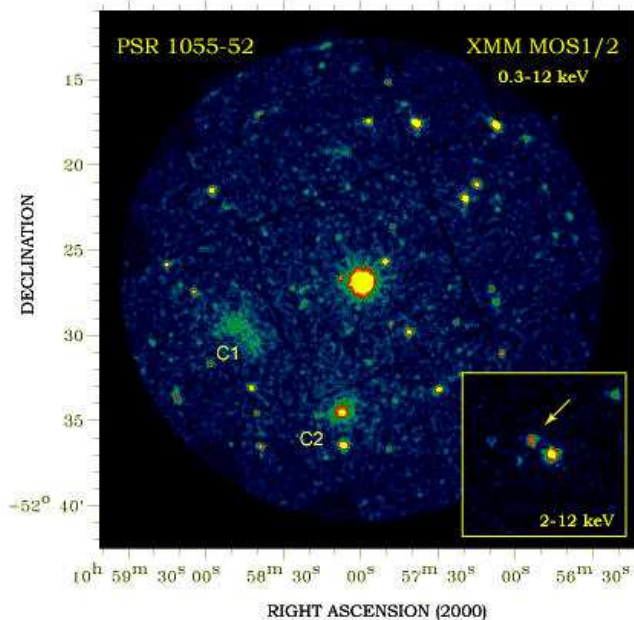


Fig. 17. The X-ray sky around PSR 1055-52 as seen by the MOS1/2 detectors in the 0.3 – 12 keV band. The inset in the lower-right corner is a zoomed view on the central $4' \times 4'$ field around PSR 1055-52 for 2-12 keV. The arrow indicates the X-ray source XMMU J105801.8-522639 which is located $\sim 30''$ offset from PSR 1055-52 which is the brightest source in the image.

eral of these sources were found to have optical and radio counterparts using the DSS2 and a radio image taken by Stappers et al. (1999) at 1.4 GHz.

The ROSAT data in the 1.0 – 2.4 keV band were quite limited as far as the photon statistics of the X-ray sources neighboring PSR 1055-52 is concerned. It was therefore of special interest so see this sky region observed by XMM-Newton, which provides a sensitivity about a factor of 10 higher than ROSAT. The X-ray sky around PSR 1055-52 as seen by XMM-Newton in the 0.3 – 12 keV band is shown in Fig.17. Apart from the many X-ray sources detected in the field the source denoted by Becker et al. (1999) as C1 appears to be extended by about 1×4 arc-minutes. Its location coincides with that of four faint radio point sources some of which have optical counterparts detected in the DSS2 (Becker et al. 1999). Similar results are found for the other putative X-ray clump C2. Interesting to note is an X-ray source located $30''$ offset from the pulsar position (cf. the inset in Fig.17). This source, denoted as XMMU J105801.8-522639, shows up only in the hard band and was not recognized in any other observation of PSR 1055-52 so far. Inspecting the data from the XMM-Newton optical monitor we found that XMMU J105801.8-522639 has no optical counterpart down to $m_v \sim 22$. The radio image of Stappers et al. (1999) shows a faint radio source near to PSR 1055-52 which roughly matches with the position

of XMMU J105801.8-522639. It might be the radio counterpart of XMMU J105801.8-522639.

5. The millisecond Pulsars

By the middle of 2002, about 100 millisecond pulsars have become known, out of which 57 are located in the galactic plane (Camilo 1999; Lommen et al. 2000; Manchester et al. 2000). The others are in globular clusters (Kulkarni & Anderson 1996; Camilo et al. 2000, D'Amico et al. 2001) which provide a favorable environment for the recycling scenario (Rasio, Pfahl & Rappaport 2000). Only 10 of the 57 galactic plane ms-pulsars are solitary (including PSR B1257+12 which has a planetary system); the rest are in binaries, usually with a low-mass white dwarf companion.

Millisecond pulsars were studied exclusively in the radio domain until the early 1990's when PSR B1957+20 was detected by ROSAT (Kulkarni et al. 1992; Fruchter et al. 1992). Unfortunately only a handful of counts were recorded from this object so that no detailed data analysis was possible. The identification was based on the positional coincidence with the radio pulsar. The first ms-pulsar with X-ray pulsations was PSR J0437-4715 (Becker & Trümper 1993). Since then further detections followed (Halpern 1996; Verbunt et al. 1996; Danner et al. 1997; Saito et al. 1997; Takahashi et al. 1999; Becker et al. 1998a; Becker et al. 1998b; Becker et al. 1999; Mineo et al. 2000, Becker et al. 2000, Grindlay et al 2002) which three years after the launch of Chandra and XMM-Newton sum up to almost 50% of all X-ray detected rotation-powered pulsars. Table 4 provides an up-to-date summary.

Although for most of these objects no detailed spectral and temporal information is available, the number of detected counts allows at least an estimate of the X-ray flux and luminosity assuming a standard X-ray spectrum (cf. Tab.4). XMM-Newton will observe several of these pulsars during AO1 (cf. Tab.2) and hopefully will provide the required spectral and temporal information to finally identify the emission mechanism responsible for the observed X-ray emission. Chandra and HST observations of the ms-pulsars detected in 47TUC are scheduled for October 2002 so that also for these objects more detailed information will become available in the near future. For the remaining pulsars, data of six objects provide sufficient spectral and/or temporal information to identify the origin of their X-ray emission (Becker & Trümper 1999 and references therein; Sakuray et al. 2001; Mineo et al. 2000). Observations by Chandra and XMM-Newton have provided the missing spectral information for some of them only recently (Kuiper et al. 2002; Zavlin et al. 2002, Becker et al. 2002c).

The X-ray emission observed from PSR B1821-24, PSR B1937+21 and PSR J0218+4232 ($P \sim 1.5 - 3$ ms, $\log \dot{E} \sim 35 - 36$ erg s^{-1}) is produced by non-thermal processes (Kawai & Saito 1999, Takahashi et al. 1998; 2001, Mineo et al. 2000, see also Nicastro et al. 2002,

Characteristics of the optical, X-ray and gamma-ray detected rotation-powered millisecond pulsars.

Pulsar	Comment	detected						$\dot{E}/(4\pi d^2)$	$\log \dot{E}$	$\log L_x^{tot}$	$\log L_x^{puls}$	$\log (P/2\dot{P})$	P	$\dot{P} \times 10^{-15}$	d	$\log B_\perp$
		R	O	X _s	X _h	γ_s	γ_h	erg/s/cm ²	erg/s	erg/s	erg/s	years	ms	s s ⁻¹	kpc	Gauss
J0437 – 4715	bin	p	-	p	-	-	-	$1.0 \cdot 10^{-9}$	33.62	30.86	30.3	9.50	5.75	$2.0 \cdot 10^{-5}$	0.18	8.54
B1937 + 21	sol	p	-	p	-	-	-	$7.1 \cdot 10^{-10}$	36.04	≤ 32.10		8.37	1.55	$1.0 \cdot 10^{-4}$	3.60	8.61
B1821 – 24	sol, M28	p	-	p	p	-	-	$6.2 \cdot 10^{-10}$	36.35	33.24		7.48	3.05	$1.6 \cdot 10^{-3}$	5.50	9.35
J0030 + 0451	sol	p	-	p	-	-	-	$5.4 \cdot 10^{-10}$	33.53	30.56	30.26	9.88	4.86	$1.0 \cdot 10^{-5}$	0.23	8.32
J2124 – 3358	sol	p	-	p	-	-	-	$4.7 \cdot 10^{-10}$	33.55	30.35	29.8	9.86	4.93	$1.1 \cdot 10^{-5}$	0.25	8.36
B1957 + 20	bin	p	-	d	-	-	-	$4.1 \cdot 10^{-10}$	35.06	31.93		9.32	1.60	$1.2 \cdot 10^{-5}$	1.53	8.14
J1024 – 0719	sol	p	-	d	-	-	-	$3.6 \cdot 10^{-10}$	33.72	29.48		9.76	5.18	$1.8 \cdot 10^{-5}$	0.35	8.49
J1744 – 1134	sol	p	-	d	-	-	-	$2.4 \cdot 10^{-10}$	33.28	29.30		9.86	4.07	$8.6 \cdot 10^{-6}$	0.26	8.27
J1012 + 5307	bin	p	-	d	-	-	-	$1.2 \cdot 10^{-10}$	33.60	30.20		9.76	5.25	$1.4 \cdot 10^{-5}$	0.52	8.45
J0218 + 4232	bin	p	-	p	-	-	?	$6.5 \cdot 10^{-11}$	35.37	32.75		8.66	2.32	$8.0 \cdot 10^{-5}$	5.85	8.63
J0751 + 1807	bin	p	-	d	-	-	-	$1.5 \cdot 10^{-11}$	33.88	31.60		9.84	3.47	$8.0 \cdot 10^{-6}$	2.02	8.23
J0024 – 7205E	bin, 47Tuc	p	-	d	-	-	-	$1.1 \cdot 10^{-11}$	34.50	30.6		≥ 8.47	3.53	$\leq 3.0 \cdot 10^{-4}$	4.60	≤ 9.00
J0024 – 7204F	sol, 47Tuc	p	-	d	-	-	-	$8.4 \cdot 10^{-12}$	34.40	30.5		≥ 8.34	2.63	$\leq 2.1 \cdot 10^{-4}$	4.60	≤ 8.90
47Tuc S	bin, 47Tuc	p	-	d	-	-	-			30.2			2.83		4.60	
J0023 – 7203J	bin, 47Tuc	p	-	d	-	-	-	$8.4 \cdot 10^{-12}$	34.40	30.3		≥ 9.15	2.10	$\leq 1.1 \cdot 10^{-4}$	4.60	≤ 8.69
J0024 – 7204O	bin, 47Tuc	p	-	d	-	-	-	$8.4 \cdot 10^{-12}$	34.40	30.6		≥ 8.38	2.64	$\leq 1.8 \cdot 10^{-4}$	4.60	≤ 8.84
J0024 – 7203U	bin, 47Tuc	p	-	d	-	-	-	$5.3 \cdot 10^{-12}$	34.20	30.3		≥ 8.60	4.34	$\leq 3.4 \cdot 10^{-4}$	4.60	≤ 9.07
J0024 – 7204N	sol, 47Tuc	p	-	d	-	-	-	$4.2 \cdot 10^{-12}$	34.10	30.2		≥ 8.81	3.05	$\leq 1.5 \cdot 10^{-4}$	4.60	≤ 8.84
J0024 – 7204I	bin, 47Tuc	p	-	d	-	-	-	$2.7 \cdot 10^{-12}$	33.90	30.2		≥ 8.72	3.48	$\leq 1.5 \cdot 10^{-4}$	4.60	≤ 8.84
J0024 – 7204G	sol, 47Tuc	p	-	d	-	-	-	$1.6 \cdot 10^{-12}$	33.70	30.1		≥ 8.69	4.04	$\leq 1.9 \cdot 10^{-4}$	4.60	≤ 8.95
J0024 – 7204D	sol, 47Tuc	p	-	d	-	-	-	$1.6 \cdot 10^{-12}$	33.70	30.3		≥ 8.83	5.75	$\leq 3.0 \cdot 10^{-4}$	4.60	≤ 9.11
J0023 – 7205M	sol, 47Tuc	p	-	d	-	-	-	$1.1 \cdot 10^{-12}$	33.50	30.1		≥ 9.51	3.67	$\leq 1.7 \cdot 10^{-4}$	4.60	≤ 8.90
J0024 – 7204H	bin, 47Tuc	p	-	d	-	-	-	$5.3 \cdot 10^{-13}$	33.20	30.1		≥ 8.88	3.21	$\leq 1.8 \cdot 10^{-4}$	4.60	≤ 8.90

Table 4. List of rotation-powered ms-pulsars that have been detected in the radio, optical, X- and/or γ -ray wavebands, ordered according to their spin-down flux density at Earth $\dot{E}/4\pi d^2$. The individual columns are as follows: 1. Pulsar name; 2. Comment: bin=binary, sol=solitary; 3-8. Energy ranges in which pulsed (p), unpulsed (d) radiation has been detected: R – radio, O – optical, X_s – soft X-rays ($E_\gamma \sim 1\text{keV}$), X_h – hard X-rays ($E_\gamma \sim 10\text{keV}$), γ_s – soft γ -rays ($E_\gamma \sim 1\text{MeV}$) and γ_h – hard γ -rays ($E_\gamma > 100\text{MeV}$). Possible detections are indicated by a question mark. \dot{E} is the pulsar spin-down power $I\Omega\dot{\Omega}$; $L_x^{tot} = 4\pi d^2 f_x$ is the sum of the pulsed and unpulsed X-ray luminosity. L_x^{puls} is the pulsed luminosity; L_x are calculated for the ROSAT energy range 0.1 – 2.4 keV. For references see Becker & Trümper (1997; 1999), Becker & Pavlov (2002) and references therein, Grindlay et al. (2002). Radio pulsar parameters have been taken from Taylor et al. (1995), Navaro et al. (1995), Bailes et al. (1997), Toscano et al. (1998), Toscano et al. (1999), Lommen et al. (2000), Camilo et al. (2000), Lange et al. (2001), van Straten et al. (2001), Freire et al. (2001). Proper motion corrected period derivatives have been used for all those pulsars for which this effect is of significance and has been measured.

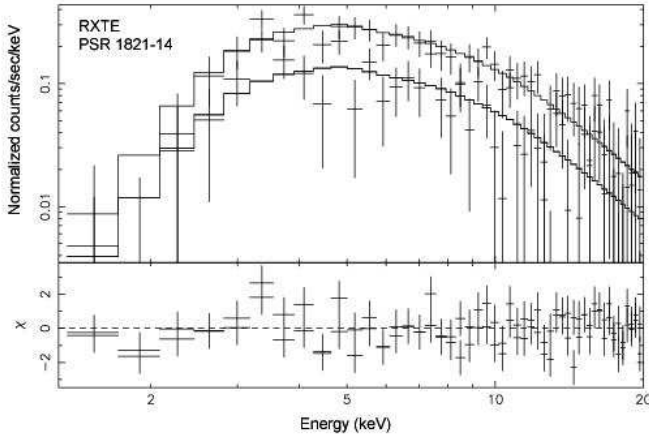


Fig. 18. X-ray spectrum of the millisecond pulsar PSR 1821-24 extracted from XTE data. A power-law spectrum yields a valid description of the data of up to 20 keV (Saito, priv. com.).

these proceedings). This is concluded from their power-law spectra (photon-index $\alpha \sim 1.5 - 2$) and pulse profiles with narrow peaks and pulsed fractions of up to $\sim 90\%$ (cf. Fig. 22). PSR B1821-24 was detected by RXTE up to ~ 20 keV (cf. Fig. 18). All these pulsars show relatively hard X-ray emission, which made it possible to study some of their emission properties already with ASCA, BeppoSAX and RXTE. For the remaining pulsars ($P \geq 4$ ms, $\log \dot{E} \sim 33 - 34$ erg s^{-1}) the X-ray emission is found to be much softer, which in the absence of definite spectral information led to the conclusion that in these pulsars thermal polar-cap emission dominates. The argument for this second group being purely thermal emitters was that their pulse profiles are broad, and that the pulsed fraction is small ($\sim 20 - 30\%$) in comparison to the non-thermal sources (pulsed fraction $\geq 50 - 60\%$). The argument is not unreasonable – thermal polar-cap emission should result in broad sinusoidally modulated soft emission with a pulsed fraction $\leq 50\%$ (Pavlov & Zavlin 1998), whereas magnetospheric emission is expected to create narrow pulse-peaks and large pulsed fractions.

But, of course, given the limited amount of data the physical interpretation is not fully justified and therefore not at all unique. Becker & Trümper (1997; 1999) have emphasized that the radiation cone confining the magnetospheric emission is likely to yield sharp peaks at one aspect angle but may be less well defined when viewed from other directions producing a less strong modulation. Thus a broad, weakly modulated pulse profile does not provide unambiguous evidence for thermal emission. Indeed, based on the L_x vs \dot{E} relation (most of the X-ray pulsars lie close to the line $L_x \sim 10^{-3} \dot{E}$, cf. Becker & Trümper 1997) one can argue on phenomenological grounds that the X-ray emission from all ms-pulsars is dominated by magnetospheric emission. The gross similarity between the X-ray and radio pulse profiles is part of this argument.

For the nearest and brightest millisecond pulsar, PSR J0437-4715, it was already evident in the ROSAT and ASCA data that the X-ray emission consists at least of two different spectral components. Either a two temperature thermal model or a model composed of a blackbody ($T \sim 1.2 \times 10^6$ K) and a power-law (photon-index $\alpha = 2.9$) fitted these data but also a broken power-law spectrum gives a valid description (Becker & Trümper 1999). The emitting area deduced from the blackbody fits was found to be very small ($R_{bb} \sim 510$ m ($d/180$ pc)), implying the existence of relatively small hot-spots on the neutron star surface from which the X-rays are emitted (Becker & Trümper 1997; 1999).

Chandra observed PSR J0437-4715 in May 2000 (Zavlin et al. 2002, cf. also Zavlin et al. and Pavlov et al., these proceedings). These data, together with the ROSAT data, provide the most significant spectral information available from this pulsar by now and suggest the presence of a power-law component and two thermal components in the pulsar's X-ray spectrum. The thermal components are interpreted as emission from a hot polar cap, having a non-uniform temperature distribution with a hot core ($T_{core} = 2.1 \times 10^6$ K, $R_{core} = 0.12$ km) and a cooler rim ($T_{rim} = 0.54 \times 10^6$ K, $R_{rim} \sim 2.0$ km). The power-law component yields a photon index of $\alpha \sim 2.2$. The size of the polar cap is found to be roughly in agreement with the theoretical predictions. Defined as the area of open field lines in which the bombardment by relativistic particles is expected, it is $R_{pc} = R(R\Omega/c)^{1/2}$. Assuming $R = 10$ km for the neutron star radius and $\Omega = 1.09 \times 10^3$ for the pulsars angular frequency $R_{pc} = 1.9$ km. It is interesting to mention that the pulsar spectrum measured by Chandra is still consistent with a broken power-law with properties similar to those fitted to ROSAT and ASCA data by Becker & Trümper (1999); $N_H = 0.3^{+0.5}_{-0.2}$ cm^{-2} , $\gamma_1 = 2.0 \pm 0.2$, $\gamma_2 = 3.6 \pm 0.1$ keV below and above the break energy $E_b = 1.1 \pm 0.1$ keV. Zavlin et al. (2002) argue against the broken power-law model because of an apparent discrepancy between the flux estimated from this model and observed by EUVE DSI - despite a known discrepancy in the cross-calibration between ROSAT and EUVE. If the broken power-law model is relevant, and this is not excluded presently by the Chandra data, it would imply that the purely non-thermal pulsar spectrum would bend down significantly in the X-ray band, which could be due to a deficit of high-energy charged particles in the pulsar's magnetosphere.

A pulsar with spin parameters similar to those observed in PSR 0437-4715 is the solitary ms-pulsar PSR 0030+0451 (cf. Table 4 and Fig.19). X-ray emission from this pulsar was discovered during the final ROSAT PSPC observations (Becker et al. 2000). Though the "dying" PSPC detector had lost most of its spectral capability a timing analysis revealed strong X-ray pulsations with a pulsed fraction of $69 \pm 18\%$. This and the gross similarity between the double peaked X-ray pulse profile and the

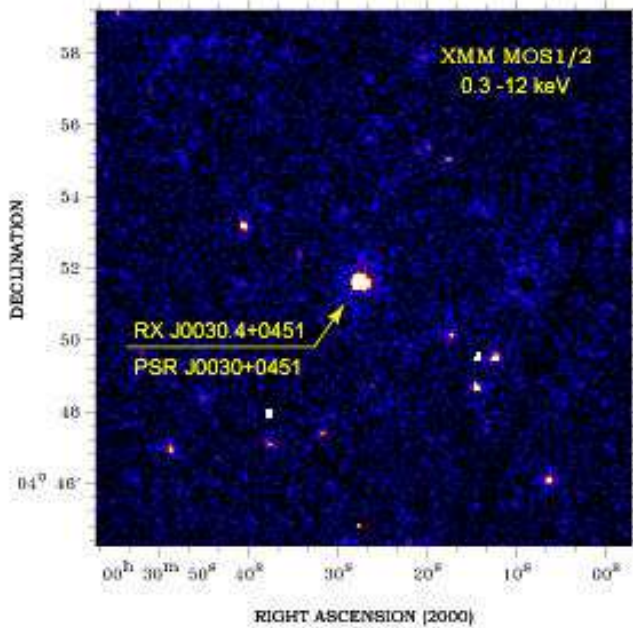


Fig. 19. The X-ray sky around PSR J0030+0451 as seen by the MOS1/2 detectors in the 0.3 – 12 keV band. The position of PSR J0030+0451 is marked. There is no evidence for any extended emission.

Crab-like radio profile taken at 1.4 GHz suggested that the X-rays from PSR 0030+0451 were most likely of non-thermal origin, although its spin-parameters appear very similar to those of PSR J0437–4715 suggesting a soft pulsar spectrum (Becker et al. 2000). It was therefore important to observe this pulsar with XMM-Newton in order to identify the emission mechanism by the spectrum rather than from just the pulse profile and the similarity of the spin-parameters with PSR J0437–4715.

PSR 0030+0451 was observed by XMM-Newton in 2001 June 19–20 for a duration of ~ 30 ksec. The MOS1/2 and the PN cameras were operated in full-frame and fast-timing mode, respectively. The latter mode required to constrain the satellite roll angle to 67–68 degrees in order to prevent source confusion in the PN data (cf. §1). The thin filters were used for the MOS1/2 and the PN cameras in order to block stray light and optical leakage from bright foreground stars. The observation is affected by several soft-proton flares covering the whole observation. Cleaning the data for the times of excessive background reduced the effective exposure time to 17.8 ksec. For the spectral analysis we selected all events in the MOS1/2 within a circle of 38 arcsec radius, containing $\sim 87\%$ of the encircled energy of a point source. The X-ray flux and luminosity were corrected accordingly. The data are not affected by pile-up.

Figure 20 shows the energy spectrum of PSR 0030+0451 observed with XMM-MOS1/2. The spectrum is rather flat in the soft band. The pulsar is detected up to ~ 7 keV. Motivated by the results obtained for PSR

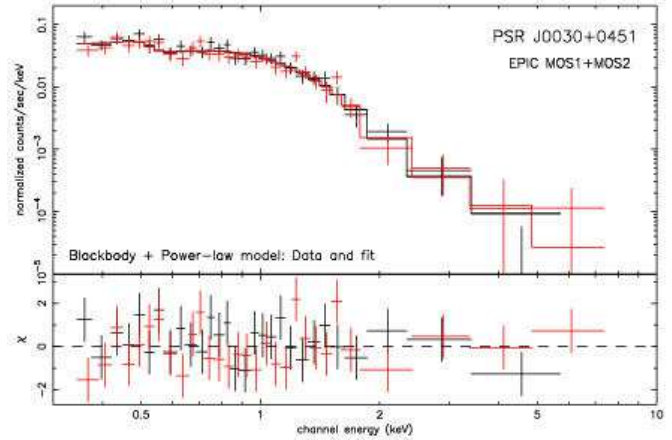


Fig. 20. X-ray spectrum of the millisecond pulsar PSR J0030+0451 extracted from XMM data. The red and black points correspond to data extracted from the MOS1 and MOS2 detectors, respectively. The data are fitted by a composite model consisting of a blackbody and power-law model. The residuals of the fits are shown at the bottom.

J0437–4715 we tested various thermal and non-thermal spectral models such as blackbody and power-law models and combinations of them as well as broken- and curved power-law spectra. A single blackbody model did not yield a valid description of the spectrum because of severe systematic deviations and a rather large reduced χ^2 of $\chi^2_\nu = 1.4$ (for 56 dof). In comparison to this, a single power-law model fits the observed spectrum ($\chi^2_\nu = 0.92$ for 56 dof) but requires a high column absorption of $N_H = (2.1 - 3.46) \times 10^{21} \text{ cm}^{-2}$ with a rather steep power-law slope of $\alpha = (4.2 - 5.1)$ for the photon-index (90% confidence range). For comparison, the column density along the pulsar’s line of sight through the entire Galaxy is just $N_H = 3 \times 10^{20} \text{ cm}^{-2}$ (Dickey and Lockman 1990). Models consisting of a combination of a blackbody and a power-law as well as of a two component blackbody model all yield an acceptable description of the observed spectrum. For the blackbody plus power-law model ($\chi^2_\nu = 0.87$ for 54 dof) we obtain $N_H = (0 - 2.5) \times 10^{20} \text{ cm}^{-2}$, $T = (2.2 - 2.7) \times 10^6 \text{ K}$, $R_{bb} = (50 - 100) \text{ m}$ and a photon index of $\alpha = 2.65 - 3.45$ (90% confidence range). The pulsar distance was assumed to be 0.23 kpc (Lommen et al. 2000). The corresponding total flux and luminosity in the 0.1–2.4 keV band is $f_x \sim 5.7 \times 10^{-13} \text{ erg s}^{-1} \text{ cm}^{-2}$ and $L_x \sim 3.6 \times 10^{30} \text{ erg s}^{-1}$. For the 0.5–10 keV band we compute $f_x \sim 1.9 \times 10^{-13} \text{ erg s}^{-1} \text{ cm}^{-2}$ and $L_x \sim 1.2 \times 10^{30} \text{ erg s}^{-1}$, respectively. The two component blackbody model fits the spectrum with comparable quality and yields $N_H = (0 - 1.9) \times 10^{20} \text{ cm}^{-2}$, $T_{bb1} = (2.6 - 3.7) \times 10^6 \text{ K}$, $T_{bb2} = (1 - 1.8) \times 10^6 \text{ K}$, $R_{bb1} = (20 - 60) \text{ m}$ and $R_{bb2} = (130 - 340) \text{ m}$. For the X-ray conversion efficiency in the 0.1–2.4 keV band we find $L_x/\dot{E} = 1.1 \times 10^{-3}$, in agreement with the general trend found by Becker & Trümper (1997). In addition to these composite mod-

els we tested a broken power-law and a curved power-law spectrum (Fossati et al. 2000) either of which provides an excellent fit to the data ($\chi^2_{\nu} = 0.93$ for 55 dof and $\chi^2_{\nu} = 0.92$ for 51 dof for the broken and curved power-law model, respectively). Fixing the column absorption to zero, we find the spectral break point at $E_b = (0.97 - 1.28)$ and photon indices of $\alpha_1 = (1.98 - 2.4)$ and $\alpha_2 = (3.88 - 5.36)$, respectively. The unabsorbed flux and luminosity obtained from this model for the 0.1–2.4 keV band are $f_x \sim (4.3 - 6.8) \times 10^{-13} \text{ erg s}^{-1} \text{ cm}^{-2}$ and $L_x \sim (2.7 - 4.3) \times 10^{30} \text{ erg s}^{-1}$, respectively. For the 0.5–10 keV band we find $f_x \sim (1.5 - 2.1) \times 10^{-13} \text{ erg s}^{-1} \text{ cm}^{-2}$ and $L_x \sim (0.95 - 1.3) \times 10^{30} \text{ erg s}^{-1}$. The fitted parameters are very similar to those found in the analysis of the Chandra data of PSR J0437-4715. Broken power-law fits thus provide an attractive alternative to describe the X-ray spectrum of PSR J0437-4715 and PSR J0030+0451 in a pure non-thermal scenario. More detailed results on the spectral analysis are presented in Becker et al. (2002c).

The rotation period of PSR J0030+0451 is 4.86 ms. The temporal resolution of the EPIC-PN camera in timing mode is 0.03 ms and thus is sufficient to measure the pulse profile and pulsed fraction as a function of photon energy. To extract the events from PSR J0030+0451 we selected an area of 8×199 pixel from the central CCD #4 of the PN camera. According to the fractional encircled energy this means that we sample about 70% of the point-spread function in x - and 100% in y -direction. Applying the usual corrections for the barycentering and the satellite orbit, a strong pulsed signal is detected in the $\sim 0.3 - 2.5$ keV band. Below and beyond that bandwidth the cumulative instrument and sky-background contribution per pixel exceeds that of the pulsar signal which prevents a detection at those energies (see Becker et al. 2002c for further details). The pulse profiles obtained from events in the 0.3–1.0 keV, 1.0–2.5 keV and 0.3–2.5 keV bands are displayed in Fig.21. Each lightcurve shows two rather narrow peaks which are separated in phase by ~ 0.5 . XMM thus confirms our findings obtained in the final ROSAT observation (Becker et al. 2000). The pulsed fraction is found to be $(49 \pm 3)\%$ in the 0.3 – 1.0 keV and $(66 \pm 12)\%$ in the 1.0 – 2.5 keV band (errors are 1σ) using a bootstrap method (Swanepoel et al.,1996). For the 0.3 – 2.5 keV bandwidth we obtain $51 \pm 3\%$. The gross similarity between the X-ray and radio pulse profiles becomes even more striking with these new pulse profiles obtained with XMM. As can be seen in Fig.22, the peak separation of the radio and X-ray lightcurves of PSR J0030+0451 appear to be in agreement with each other, suggesting a close relation between the X-ray and radio emission mechanism. It is evident that this holds for all the other pulse profiles shown in the chart. It is straight forward to understand this gross similarity in terms of a common non-thermal emission mechanism but it is hard to understand how a mixture of thermal and non-thermal emission mechanisms can produce this similarity. In the case of PSR J0437-4715,

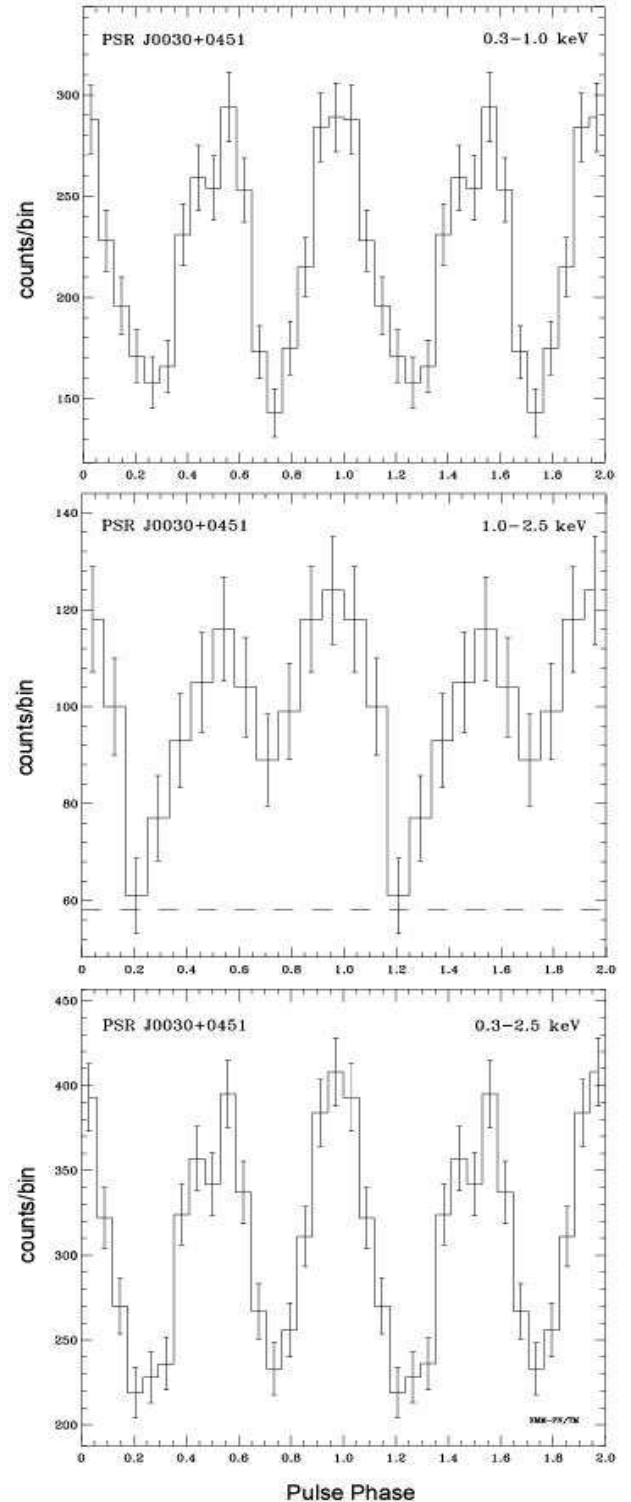


Fig. 21. Pulse profiles of PSR J0030+0451 observed by XMM-Newton. Two full pulse cycles are shown for clarity. The profile appears double peaked with a pulsed fraction of $50 \pm 3\%$ in the 0.3 – 2.5 keV band.

for which the *broad* X-ray pulse profile often is taken as an additional argument for the thermal origin of its soft X-radiation, it should be noted that also the radio emission

has a duty cycle of $\sim 80\%$ so that the radio pulse itself appears rather broad.

In the light of these new results it will be interesting to see the data from more millisecond pulsars observed by XMM-Newton and Chandra in order to further explore these interesting objects and their emission mechanisms.

6. Concluding remarks

In spite of the first impressive achievements summarized above, lots of questions still remain. First, the evolution of neutron stars, beginning with their violent birth in supernova explosions, is far from being well understood. Until recently, a common prejudice had been that all neutron stars are born as active, fast spinning rotation-powered pulsars, which slow down their rotation, eventually stop their activity and, after crossing a “death line”, get into the “pulsar graveyard”. A former pulsar remains in the graveyard forever, cool and quiet, unless it is captured by a flying-by star (e.g., in a globular cluster) and forms a close binary, where accretion onto the neutron star can spin it up (recycle) to periods that short that it again becomes an active pulsar. However, as the results from XMM-Newton and Chandra have shown, it is likely that the picture is not as simple as that. In particular, it appears that several very young neutron stars (like those in Puppis-A and RCW 103) are not active pulsars at all. Others are found to have spin periods longer than the canonical limit of 4 seconds. Were those objects born with such a slow spin-period or did they spin down rapidly after their formation because of the presence of an ultra-strong magnetic field? Or is it simply an unfavorable beaming which precludes to see the pulsed emission? Since such objects are not seen in radio, and are extremely faint in optical, they could not be observed until the onset of the X-ray astronomy era, which means that our perception of neutron star early evolution was strongly biased in favor of much easier observable radio pulsars. Why are many (perhaps, the majority of) nascent neutron stars not active pulsars? Is it because they are indeed magnetars, whose super-strong magnetic field inhibits the pulsar activity? Or, on the contrary, are their magnetic fields so weak and/or is their rotation so slow that the pulsar does not turn on? Or is their pulsar activity quenched by accretion of debris of the supernova explosion? Are the (apparently young) anomalous X-ray pulsars and soft gamma-ray repeaters indeed magnetars or are their unusual observational properties due to quite different reasons, like a residual disk?

Observing middle aged neutron stars at X-ray energies has provided valuable information on the pulsars’ surface temperature for some objects. The XMM data have provided further evidence that the surface temperature distribution is not uniform and several, at least two, thermal components are required to describe the observed spectra. The question remains what mechanisms are responsible for the non-uniform surface temperature distribution?

Is the presence of the strong magnetic field already sufficient to channel the heat flow in the star to produce the observed non-uniformity, or is it due to the presence of polar caps which are heated by a bombardment of energetic particles accelerated in the neutron star’s magnetosphere? Other questions are related to the chemical composition of the neutron star surface layer and the presence of a neutron star atmosphere. Why does none of the data taken so far show any direct evidence for the existence of a neutron star atmosphere except 1E1207-5209 (cf. Pavlov et al., these proceedings; Mereghetti et al., 2002 and references therein)? No emission or absorption features are observed in the LETG spectrum taken from the nearby isolated neutron star RX J1856-3754, but a blackbody was measured with very high accuracy (Burwitz et al. 2001; cf. Pavlov et al., these proceedings).

Crucial for building a consistent evolutionary scenario of pulsar emission properties at X-ray energies are older pulsars in the age bracket $10^6 - 10^7$ years. What is the dominant emission process producing their X-rays? Only a few of these objects turn out to be bright enough to be observable at all. None of them has been observed by XMM-Newton or Chandra so far but a few objects are scheduled for XMM’s AO1 (cf. Tab.2). These pulsars are of particular importance for the study of particle acceleration and high energy radiation processes on the neutron star surface and in the magnetosphere. This is because of their outstanding location in the $P - \dot{P}$ parameter space, where they are found in the area of strong magnetic fields ($\sim 10^{11} - 10^{12}$ G) but spin-down ages which are intermediate between the middle aged cooling neutron stars and the very old $\sim 10^9 - 10^{10}$ years millisecond pulsars. Will the thermal emission observed in cooling neutron stars simply fade away with increasing age due to the neutron star cooling or will the star be kept hot at about $(0.5 - 1) \times 10^5$ K over millions of years due to energy dissipation by processes such as internal frictional heating ($\dot{E}_{diss} \sim 10^{28} - 10^{30}$ erg/s) and crust cracking or by vortex pinning and creeping?

As far as millisecond pulsars are concerned, what are the pulsar parameters which determine the relative strength of the thermal and non-thermal emission components? Or is the pulsar emission non-thermal for all detected objects? Why do the pulse profiles observed in the radio and X-ray bands show this strong gross similarity, even when their X-ray emission appears to be emitted mainly from heated polar-caps like proposed for PSR J0437-4715? What is causing the relation between the emission properties and energy spectra, which is observed in the radio and X-ray band?

In this paper we have shown that observatories like XMM-Newton provide very exciting new results on all classes of neutron stars and that this observatory will be able to provide the answer for many of the open questions mentioned above. We are confident that XMM-Newton and Chandra will have a similar strong impact on our

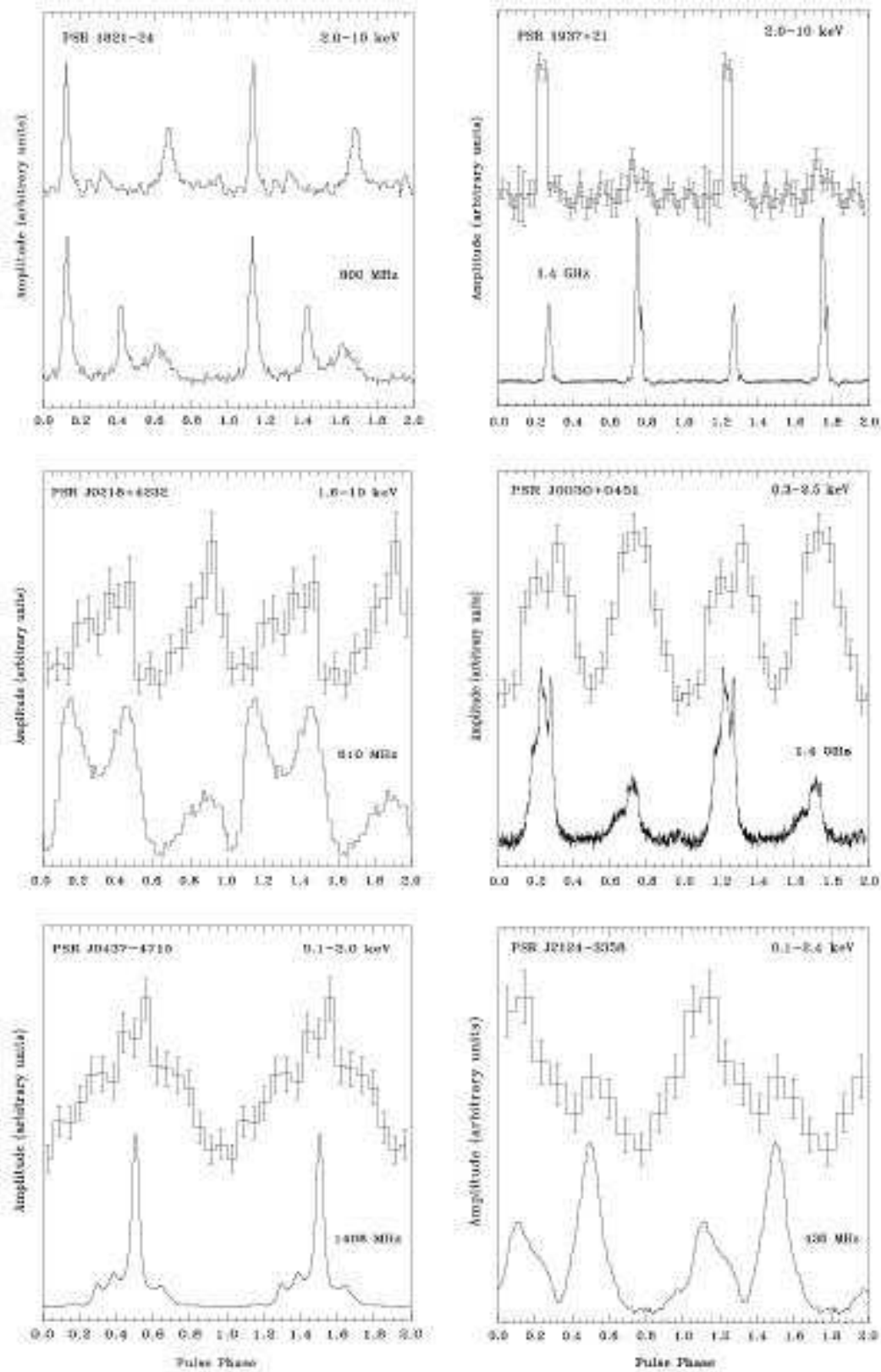


Fig. 22. Integrated lightcurves for all ms-pulsars for which X-ray pulses have been detected. The upper panel phase histograms show the pulse profiles for the energy bands noted. The radio profiles are shown in the lower panel for comparison. Two full pulse cycles are shown for clarity. The relative phase between the radio and X-ray pulses is only known for PSR 1821-24, B1937+21, 0218+4232 and PSR J0437-4715. The phase alignment in all other cases is arbitrary due to the lack of accurate clock calibration.

understanding of neutron star emission mechanisms as ROSAT had few years ago. With respect to this it might be worth to mention that we still use the soft photons detected by ROSAT to explore the X-ray spectra of pulsars because none of the new instruments can compete in the soft band down to energies of 0.1 keV.

Acknowledgements. We would like to thank the XMM team at ESTEC and MPE for their help with the data analysis, especially Dirk Grupe for the compilation of the data analysis cookbook and Michael Freyberg for his help during the data processing and analysis. Uwe Lammers, Eckhard Kenziora, Markus Kuster, Tim Oesterbroek and Ed Serpell for the help with the clock calibration. WEB is thankful for discussion with M.Weisskopf and J.Grindlay.

References

- Aschenbach, B., 1998, *Nat*, 396, 141
- Aschenbach, B., Iyudin, A., Schönfelder, V., 1999, *A&A*, 350, 997
- Bailes, M., Johnston, S., Bell, J.F., et al, 1997, *ApJ*, 481, 386
- Becker, W., & Trümper, J. 1993, *Nat*, 365, 528
- Becker, W., Trümper, J., Hasinger, G., Aschenbach, B., 1993, in *Isolated Pulsars*, eds. K.A. Van Riper, R.I. Epstein & C. Ho, p116, Cambridge University Press
- Becker, W., Trümper, J., 1997, *A&A*, 326, 682
- Becker, W., Trümper, J., 1998a, *IAU Circular No. 6829*
- Becker, W., Trümper, J., Hasinger, G., 1998b, *IAU Circular No. 6845*
- Becker, W., Trümper, J. 1999, *A&A*, 341, 803
- Becker, W., Kawai, N., Brinkmann, W., Mignani, R., 1999, *A&A*, 352, 532
- Becker, W., Trümper, J., Lommen, A.N., Backer, D.C., 2000, *ApJ*, 545, 1015
- Becker, W., 2001, Talk presented at the second XMM Symposium *New Vision of the X-ray Universe in the XMM-Newton and Chandra Era*, Nov. 2001, ESTEC
- Becker, W., Pavlov, G.G., 2002, in *The century of Space Science*, eds. J.Bleeker, J.Geiss & M.Huber, Kluwer Academic Press, in press, astro-ph/0208356
- Becker, W., Aschenbach, B., Iyudin, A., 2002a, *A&A*, submitted
- Becker, W., et al., 2002b, *A&A*, submitted
- Becker, W., et al., 2002c, *ApJ*, submitted
- Burwitz, V., Zavlin, V.E., Neuhäuser, R., Predehl, P., Trümper, J., Brinkman, A. C., 2001, *A&A*, 379, 35L
- Camilo, F. 1999, in *Pulsar Timing, General Relativity and the Internal Structure of Neutron Stars*, ed. Z. Arzoumanian, F. Van der Hooft, & E.P.J. van den Heuvel, Amsterdam: Koninklijke Nederlandse Akademie van Wetenschappen, p. 115
- Camilo, F., Lorimer, D. R., Freire, P., Lyne, A. G., & Manchester, R. N., 2000, *ApJ*, 535, 975
- Caraveo, P.A., Mignani, R., Pavlov, G.G., Bignami, G.F., 2002, in *A decade of HST science*, Space Telescope Science Institute Symposium, eds. M.Livio, K.Noll and M.Stiavell, p13
- Cheng, K.S., Ho, C. & Ruderman, M.A., 1986, *ApJ*, 300, 500
- Danner R., Kulkarni S.R., Saito Y., Kawai N., 1997, *Nat* 388, 751
- D'Amico, N., Lyne, A.G., Manchester, R.N., Possenti, A., Camilo, F., 2001, *ApJ*, 548, L171
- Dickel, J.R., Carter, L.M., *Memorie della Societa Astronomia Italiana*, Vol. 69, p.845
- Dickey J. M., Lockman F. J., 1990, *ARA&A*, 28,215
- Freire, P.C., Camilo, F., Lorimer, D.R., Lyne, A.G., Manchester, R.N., D'Amico, N., 2001, *MNRAS*, 326, 901
- Fruchter A.S., Bookbinder J., Garcia M.R., Bailyn C.D., 1992, *Nat*, 359, 303
- Fossati, G., Celotti, A., Chiaberge, M., et al., 2000, *ApJ*, 541, 166
- Garmire, G.P., Pavlov, G.G., Garmire, A.B., Zavlin V.E. 2000, *IAU Circ. #7350*
- Green, A.,2000, *A Catalogue of Galactic Supernova Remnants*, Mullard Radio Astronomy Observatory, Cambridge, UK
- Greiveldinger, C., Camerini, U., Fry, W., et al. 1996, *ApJ*, 465, L35
- Grindlay, J.E., Camilo, F., Heinke, C.O., Edmonds, P.E., Cohn, H., Lugger, P., 2002, to appear in *ApJ*
- Gotthelf, E.V., Petre, R., Vasisht, G. 1999a, *ApJ*. 514, L107
- Halpern, J.P., Holt, S.S., 1992, *Nat*, 357, 222
- Halpern J.P., 1996, *ApJ*, 459, L9
- Harding, A.K., Muslimov, A.G., 2002, *ApJ*, 568, 862
- in't Zand, J.J.M., et al.,1998, *A&A*, 331, L25
- Iyudin, A.F., Schönfelder, V., Bennett, K., Bloemen, H., Diehl, R., Hermsen, W., Lichti, G.G., van der Meulen, R.D., Ryan, J., Winkler, C., 1998, *Nat*, 396, 142
- Johnston S., Lorimer D.R., Harrison P.A., et al. 1993, *Nat*, 361, 613
- Kawai, N., Tamura, K., 1996, in *IAU Colloquium 160*, eds S.Johnston, M.A.Walker and M.Bailes, p367
- Kawai, N., Saito, Y., 1999, *Astro. Lett. and Communications*, 38, 1
- Kaspi, V.M., Crawford, F., Manchester, R.N., Lyne, A.G., Camilo, F., D'Amico, N., Gaensler, B.M., 1998, *ApJ*, 503, L161
- Kendziorra E., Kuster, M., Kirsch, M., Risse, P., Straubert, R., Becker, W., Strüder L., Treis, J., Lechner, P., Holl, P., 2002, *SPIE Conference 4851*,
- Kuiper, L., Hermsen, W., Verbunt, F., Ord, S., Stairs, I., Lyne, A., 2002, *ApJ*, in press, astro-ph/0206081
- Kulkarni, S. R., Anderson, S. B. 1996, in *Dynamical Evolution of Star Clusters – Confrontation of Theory and Observations*: IAU Symposium 174, Kluwer Academic Publisher, p.181
- Kulkarni S.R., Phinney E.S., Evans C.R., Hasinger G., 1992, *Nat*, 359, 300
- Kuster, M., Kendziorra, E., Benlloch, S., Becker, W., Lammers, U., Vacanti, G., Serpell, E., 2002, in the Proceedings of *New Vision of the X-ray Universe in the XMM-Newton and Chandra Era*, Nov. 2001, ESTEC, in press
- Lange, C., Camilo, F., Wex, N., Kramer, M., Backer, D.C., Lyne, A.G., Doroshenko, O., *MNRAS*, 326, 274
- Lyne, A.G., Jordan, C.A., Roberts, M.E., 2002, *Jodrell Bank Crab Pulsar Timing Results*, Monthly Ephemeris, University of Manchester
- Lommen, A.N., Zepka, A., Backer, D.C., Cordes, J.M., Arzoumanian, Z., McLaughlin, M., & Xilouris, K. 2000, *ApJ*, 545, 1007
- Manchester, R. N., Lyne, A. G., Camilo, F., Kaspi, V. M., Stairs, I. H., Crawford, F., Morris, D. J., Bell, J. F., &

- D'Amico, N., 2000, in *Pulsar Astronomy - 2000 and Beyond*, ed. M.Kramer, N.Wex, and R.Wielebinski, San Francisco: ASP, p.49
- Manchester et al., 2002, Catalog of pulsars, unpublished
- Marshall, H.L., Schulz, N.S., 2001, AAS, 199, #119.05
- Mereghetti, S., 2001, ApJ, 548, L213
- Mereghetti, S., De Luca, A., Caraveo, P.A., Becker, W., Mignani, R., Bignami G.F., 2002, accepted for ApJ, astro-ph/0207296
- Mineo, T., Cusumano, G., Kuiper, L., Hermsen, W., Massaro E., Becker, W., Nicastro, L., Sacco, B., Verbunt, F., Lyne, A.G., Stairs, I.H., Shibata, S. 2000, A&A, 355, 1053
- Navaro, J., de Bruyn, G., Frail, D., Kulkarni, S.R., Lyne, A.G., 1995, ApJ, 455, L55
- Ögelman, H., Finley, J.P., 1993, ApJ, 413, L31
- Ögelman, H.B., 1995, in *The Lives of Neutron Stars*, eds M.Alpar et al., NATO ASI Series Vol. 450, Kluwer Academic Publisher, p101-120
- Paerels, F., Mori, K., Motch, C., Haberl, F., Zavlin, V.E., Zane, S., Ramsay, G., Cropper, M., Brinkman, B., 2001, A&A, 365, 298L
- Pavlov, G.G., Shibano, Y.A., Zavlin, V.E., 1995, in *The Lives of Neutron Stars*, eds. A.Alpar, U.Kilizoglu & J. van Paradijs, Kluwer Academic Publishers, p71
- Pavlov, G.G., Sanwal, D., Kiziltan, B., G.Garmire, 2001, ApJ, 559, 131
- Petre, R. Becker, C.M., Winkler, P.F. 1996, ApJ, 465, L43
- Potekhin, A., Yakovlev, D., 2001, A&A, 374, 213
- Rajagopal, M., Romani, R.W. 1996, ApJ, 461, 327
- Rasio, F.A., Pfahl, E.D., & Rappaport, S. 2000, ApJ, 532, L47
- Rots, A.H., Jahoda, K., Lyne, A.G., 2000, AAS, HEAD meeting #32, #33.08
- Saito Y., Kawai N., Kamae T., et al., 1997, ApJ, 477, L37
- Saito, Y., 1998, Ph.D. thesis, Tokio Univ. (ISAS Research Note 643)
- Sakurai, I., Kawai, N., Torii, K., Negoro, H., Nagase, F., Shibata, S., Becker, W., 2001, PASJ, 53, 535
- Sanwal, D., et al., 2002, AAS 200, 7201
- Slane, P., Hughes, J.P., Edgar, J., et al., 2001, ApJ, 548, 814
- Stappers, B.W., Gaensler, B.M., Johnston S., 1999, MNRAS, 308, 609
- Swanepoel J.W.H., de Beer C.F., Loots H., 1996, ApJ, 467, 261
- Takahashi M., Shibata S., Torii K., Saito Y., Kawai N. 1998, IAU Circ. 7030
- Takahashi, M., Shibata, S., Torii, K., Saito, Y., Kawai, N., Hirayama, M., Dotani, T., Gunji, S., Sakurai, H., Stairs, I.H., Manchester, R.N., 2001, ApJ, 554, 316
- Tennant, A.F., Becker, W., Juda, M., Elsner, R.F., Kolodziejczak, J.J. Murray, S.S., O'Dell, S.L., Paerels, F., Swartz, D.A., Shibasaki, N., Weisskopf, M.C., 2001, ApJ, 554, L173
- Torii, K., 1998, Ph.D. thesis, Osaka Univ. (ISAS Research Note 650)
- Torii, K., Kinugasa, K., Toneri, T., Asanuma, T., Tsunemi, H., Dotani, T., Mitsuda, K., Gotthelf, E. V., Petre, R., 1998, ApJ, 494L, 207
- Torii, K., Gotthelf, E.V., Vasisht, G., Dotani, T., Kinguasa, K., ApJ, 2000, 534, L71
- Toscano, M., Bailes, M., Manchester, R., Sandhu, J.S., 1998, ApJ, 506, 863
- Toscano, M., Britton, M.C., Manchester, R., Bailes, M., Sandhu, J.S., Kulkarni, S., Anderson, S.B., 1999, ApJ, 523, L171
- Tsunemi, H., Miyata, E., Aschenbach, B., Hiraga, J., Akutsu, D., 2000, PASJ, 52, 887
- Tuohy, I.R., Garmire, G.P. 1980, ApJ, 239, L107
- van Straten, W., Bailes, M., Britton, M., Kulkarno, S.R., Anderson, S.B., Manchseter, R.N., Sarkissian, J., 2001, Nat, 412, 158
- Verbunt F., Kuiper L., Belloni T., et al, 1996, A&A, 311, L9
- Wijnands, R., van der Klis, M., 1998, Nat, 394, 344,
- Weisskopf, M.C., Hester, J.J., Tennant, A.F., et al. 2000, ApJ, 536, L81
- Willingale, R., Aschenbach, B., Griffiths, R. G., Sembay, S., Warwick, R. S., Becker, W., Abbey, A. F., Bonnet-Bidaud, J.-M., 2001, A&A, 365, L212
- Zavlin, V.E., Pavlov, G.G., Shibano, Y.A., 1996, A&A, 315, 141
- Zavlin, V.E., Trümper, J., Pavlov, G.G., 1999, ApJ, 525, 959
- Zavlin, V.E., Pavlov, G.G., Sanwal, D., Manchester, R.N., Trümper, J., Halpern, J.P., Becker, W., 2002, ApJ, 569, 894